

Atom-Photon Entanglement

Diplomarbeit

im Studiengang Diplom Physik
angefertigt an der Fakultät für Physik
der Ludwig-Maximilians-Universität München
Arbeitsgruppe Prof. Dr. Harald Weinfurter

von

Norbert Ortegel

München, den 06. Juli 2009

Erstgutachter: Prof. Dr. H. Weinfurter
Zweitgutachter: Dr. F. Marquardt

”Wenn es bei dieser verdammten
Quantenspringerei bleiben soll,
so bedaure ich, mich mit der
Quantentheorie überhaupt befaßt zu haben”

Erwin Schrödinger

Contents

1	Introduction	1
2	Concepts of atom-photon and atom-atom entanglement	5
2.1	Theoretical description	5
2.1.1	Two-level systems	5
2.1.2	Entanglement of two-qubit systems	7
2.1.3	Fidelity	8
2.2	Atom-photon entanglement with ^{87}Rb	10
2.2.1	Creation of entanglement	10
2.2.2	Definition of the measurement bases	11
2.3	Entanglement of two remotely trapped atoms	13
2.3.1	Entanglement swapping	13
2.3.2	Two-photon interference	14
2.4	Tests of Bell's inequality	15
2.4.1	Loopholes	16
2.4.2	Technical requirements for a loophole-free Bell-test with two ^{87}Rb -atoms	17
3	Experimental realization of atom-photon entanglement	19
3.1	Technical components	19
3.1.1	Laser system	19
3.1.2	Pattern generator	20
3.1.3	Recording of events	21
3.2	Single atom trap	22
3.2.1	Vacuum system	22
3.2.2	Magneto-optical trap	22
3.2.3	Optical dipole trap	23
3.3	Overview of the experimental procedure	26
3.4	Readout of the atomic state	29
3.4.1	Hyperfine state detection	29
3.4.2	STIRAP for a three-level system	30
3.4.3	Zeeman state-selective STIRAP	32
3.4.4	Experimental realization of STIRAP	33
3.5	Stabilization of the atomic qubit	37

3.5.1	Mechanisms of dephasing	37
3.5.2	Method for compensation of external magnetic fields	39
3.5.3	Evolution of a spin-1 system in a constant magnetic field	40
3.5.4	Measurements of Larmor precessions	44
3.6	Optimization of the optical pumping duration	46
3.7	Creation of entanglement	47
3.7.1	Temporal shape of the excitation pulse and the emitted photons	48
3.7.2	Optimal pulse intensity	49
3.7.3	Creating spectrally indistinguishable photons	51
3.8	Measurement of atom-photon correlations	55
3.8.1	Choice of the measurement bases and expected correlations	55
3.8.2	Experimental sequence	56
3.8.3	Results	57
4	Temperature measurement of a single trapped atom	63
4.1	Method	63
4.2	Theoretical model	65
4.3	Results	67
5	Summary and outlook	71
A	Appendix	73
A.1	Rubidium 87 data	73
A.2	Saturation intensities	74
	Bibliography	75

1 Introduction

“Can quantum mechanical description of physical reality be considered complete?”

[1] This is the question that Einstein, Podolsky and Rosen raised in their famous publication of the so-called EPR-paradox in 1935. In order to find an answer to this question they assumed two fundamental concepts to be true. First the concept of *locality* which says that it is possible to separate two particles such that a measurement on one particle cannot influence a measurement on the other particle. And second the paradigm of *realism*. This states that every quantity that can be measured at a physical system has a predefined value already before the measurement is performed. Starting from these assumptions they derived that the quantum mechanical description of reality is *incomplete*. As many physicists of their time Einstein, Podolsky and Rosen were shaped by the classical deterministic theories of physics such as Newtonian mechanics and Maxwell’s electrodynamics. They therefore doubted that quantum mechanics with its probabilistic nature should be the final theory to describe the physical world. *“We believe, however, that such a [complete and deterministic] theory is possible.”*[1] they closed their considerations. This idea inspired so-called *local hidden variable* (LHV) theories. These theories suppose that additional parameters exist which are unaccessible in experiment but which predetermine the outcomes of measurements on quantum mechanical systems.

The argumentation in the EPR-paradox was based on a gedanken experiment with two particles that are entangled in their position- and momentum degrees of freedom. Einstein, Podolsky and Rosen exploited the non-classical correlations that arise between the outcomes of simultaneous measurements on such entangled particles, even if they are space-like separated. A realization of this gedanken experiment seemed impossible until Bohm proposed an equivalent experiment using two entangled spin- $\frac{1}{2}$ particles [2]. In 1964 J.S. Bell discovered [3] how such an experiment can help to decide the question whether quantum mechanics already gives a complete description of nature or whether there exist additional local hidden variables. He formulated an inequality for the measurement outcomes on an entangled two-particle system that should always hold if local hidden variables existed, but which is violated by quantum mechanical predictions. In the following decades experiments reproduced the predictions of quantum mechanics [4, 5, 6, 7] and thus gave an indication that LHV theories might be wrong.

However, all of these experiments left open so-called *loopholes* that still allow for a local realistic description of nature. First, the measurements on the entangled

particles were not space-like separated. Thus, it was not guaranteed that the measurements were causally independent from each other. This *locality loophole* could be closed by using entangled pairs of photons that were first separated by a sufficiently long distance before the measurements were performed [8]. Second, it is necessary to detect a certain minimal fraction of the whole ensemble of entangled pairs that are created during such an experiment. Otherwise it must be assumed that the detected pairs are representative for the whole ensemble. In experiments with photons this could not be achieved due to the low quantum efficiencies of photon detectors. In contrast, experiments with entangled ions [9, 10] were able to close this *detection loophole* due to the high detection efficiency for massive particles. Here, however, the measurements were again not spacelike separated.

The aim of our group is to build a system that is capable of closing both loopholes simultaneously. Its major building blocks are two neutral ^{87}Rb atoms that are trapped at remote locations separated by 300 m. Entanglement between the atoms can be established by using the entanglement swapping protocol [11]. For this each of the atoms is first entangled with a photon. The photons are then brought together and a Bell-state measurement is performed on the two-photon state by interference of the photons on a beamsplitter. By this procedure the entangled photon state is transferred onto the atoms. Given a method to perform a projection measurement on both atoms within less than $\frac{300\text{ m}}{c} = 1\ \mu\text{s}$, a violation of Bell's inequality with spacelike separated measurements becomes possible. In this scheme the detection of the photons in the Bell-state measurement “heralds” each entangled atom-atom pair. Therefore our approach allows the so-called “even-ready scheme” [12] that - combined with the high detection efficiency of massive particles - allows to read out *every* entangled atom-atom pair. Hence, it is possible to close the detection loophole as well.

Atom-photon entanglement is the key technique for realizing this test of Bell's inequality. Such a hybrid entangled system between particles of different species allows to exploit the advantages of atoms and photons at the same time.

Hybrid entangled systems also find applications in the field of quantum information. Trapped neutral atoms or ions with their relatively long coherence times of several μs up to ms are candidates for quantum memories to store quantum information. At the same time photons are able to transmit quantum information between different locations. In this context atom-photon entanglement can serve as an interface between atomic quantum memories and photonic quantum channels. In particular, a system of two remotely trapped atoms entangled by means of the entanglement swapping protocol as described above forms one of the necessary components for so-called quantum repeaters [13]. These are the major building blocks to perform quantum communication over long distances.

As a first step towards an entangled pair of atoms at remote locations, atom-photon entanglement has already been realized in our group [14]. The single ^{87}Rb atom was stored in an optical dipole trap. In a spontaneous decay its Zeeman state was entangled with the polarization state of a single photon that was emitted during the decay process. Moreover, it was demonstrated that the emitted photon can be distributed over a 300 m long optical fiber without loss of entanglement between the atom and the photon [15].

Meanwhile a second single atom trap has been constructed in a laboratory at about 30 m distance from the first setup [16, 17, 18]. Subject of the present work is to generate and verify entanglement between the trapped atom and a single photon in this second trap setup.

Overview

At the beginning of this work the notions for describing two level systems are introduced together with the basic properties of entangled states of two level systems. Thereafter the process of generating the entangled atom-photon state in a spontaneous decay of the atom is explained. Afterwards a brief overview of atom-atom entanglement via entanglement swapping will be given. It will be addressed which technical requirements the setups for atom-photon entanglement have to fulfill in order to perform the envisaged loophole-free Bell-test.

The main chapter of this work presents the experimental realization of the steps that are necessary to create an entangled atom-photon pair and to verify the entanglement of the two-particle state. This involves trapping of a single ^{87}Rb atom in an optical dipole trap, readout of the atomic Zeeman state as well as stabilization of the atomic state against external magnetic fields. Besides, an efficient preparation of the atom in the excited state from where the sponaneous decay takes place is crucial in order to achieve a high generation rate of entangled atom-photon pairs. It will be demonstrated that it is possible to switch off the trapping potential during this excitation process. By these means it can be achieved that the photons emitted from the two remote atoms are spectrally identical - a necessary condition for an efficient Bell-state measurement of the two photons. Finally, it will be shown that measurements on the created atom-photon state yield non-classical correlations that prove that the two-particle state is entangled.

In the last chapter a method is introduced by which it is possible to measure the temperature of a single atom in an optical dipole trap. Besides the general interest in the thermal properties of a single atom, its energy distribution also plays a role for broadening of the atomic transition lines.

2 Concepts of atom-photon and atom-atom entanglement

This chapter first introduces the theoretical notions which are necessary to describe quantum mechanical two-level systems and entanglement between them. Afterwards it will be explained how entanglement between a single ^{87}Rb atom and a single photon can be created in a Λ -type spontaneous decay. The future goal of the present work is to use atom-photon entanglement as a tool for generating entanglement between remotely trapped ^{87}Rb -atoms via entanglement swapping. The scheme for realizing this is presented in the third section of this chapter. In the end, Bell's inequality will be introduced as a tool for testing local hidden variable theories and it will be discussed which technical requirements must be fulfilled in order to be able to perform a loophole free test of Bell's inequality with a pair of entangled ^{87}Rb atoms.

2.1 Theoretical description

2.1.1 Two-level systems

A two-level system is defined as a physical system that has a 2-dimensional Hilbert-space. In quantum information and quantum computing science such a system is usually referred to as a *qubit* - the quantum analogon of a classical bit. Examples are the polarization states of photons or a magnetic spin- $\frac{1}{2}$ -system such as an electron, a neutron or Ag-atoms as they were used in the original Stern-Gerlach experiment. In the case of atoms or ions two different energy levels can span a 2-dimensional Hilbert-space. For our ^{87}Rb -atoms the qubit-space will be given by two Zeeman-sublevels of the $5^2S_{1/2}, F = 1$ hyperfine ground-state.

In Dirac's Bra-Ket notation a general representation of the pure state of a two-level system with eigenstates $\{|0\rangle, |1\rangle\}$ is given by:

$$|\Psi(\theta, \phi)\rangle = \cos \frac{\theta}{2} |0\rangle + e^{i\phi} \sin \frac{\theta}{2} |1\rangle \quad (2.1)$$

With $\theta \in [0, \pi]$, $\phi \in [0, 2\pi]$.

The observables for measurements on such a qubit are the Pauli operators $\hat{\sigma}_x, \hat{\sigma}_y, \hat{\sigma}_z$ with the eigenbases $\{|0_i\rangle, |1_i\rangle\} (i \in \{x, y, z\})$ and eigenvalues ± 1 . Throughout this work the qubit states under consideration will be represented in the basis of $\hat{\sigma}_z$. The representations of the eigenstates of $\hat{\sigma}_x$ and $\hat{\sigma}_y$ in terms of the basis states of $\hat{\sigma}_z$ are:

$$\begin{aligned} |0\rangle_x &= \frac{1}{\sqrt{2}} (|0\rangle_z + |1\rangle_z) \\ |1\rangle_x &= \frac{1}{\sqrt{2}} (|0\rangle_z - |1\rangle_z) \\ |0\rangle_y &= \frac{1}{\sqrt{2}} (|0\rangle_z + i|1\rangle_z) \\ |1\rangle_y &= \frac{1}{\sqrt{2}} (|0\rangle_z - i|1\rangle_z) \end{aligned} \tag{2.2}$$

The three Pauli operators do not commute with each other. Therefore, if a system is in the eigenstate of one of the Pauli operators, a measurement on it in a basis of another Pauli operator gives entirely random outcomes.

Considering the polarization states of photons, the three pairs of eigenstates of the Pauli operators are, for example, linear horizontal and vertical polarization (H, V), linear polarization at $\pm 45^\circ$ and right and left circular polarization (σ^+, σ^-). Considering a spin- $\frac{1}{2}$ system, the three pairs of eigenstates are given by spin orientation parallel and antiparallel to the three spatial axes. In an experiment one must define a reference frame for the setup such that the pair of binary measurement outcomes for each of the three measurement settings is attributed to one of the eigenbases of the Pauli-operators. This will be done for our case of atoms and photons in section 2.2.2.

Representation on the Bloch-Sphere

An illustrative graphical representation of the state $|\Psi\rangle$ of a two-level system is given by the so called Bloch-sphere (see figure 2.1). Here we take the three dimensional unit sphere and define the pairs of unit vectors along the directions of the three spatial axes to be the representation of the three basis pairs of $\hat{\sigma}_x, \hat{\sigma}_y$ and $\hat{\sigma}_z$, respectively. The general state $|\Psi(\theta, \phi)\rangle$ (eq. 2.1) represented in the basis of σ_z is then given by a vector pointing from the origin to a certain point on the surface of the sphere as depicted in the figure.

This graphical representation becomes very useful when considering unitary transformations on qubits. In an experiment this can be, for example, the action of birefringent optical elements on the polarization states of photons or the action of a magnetic field that causes a spin- $\frac{1}{2}$ system to perform Larmor precessions.

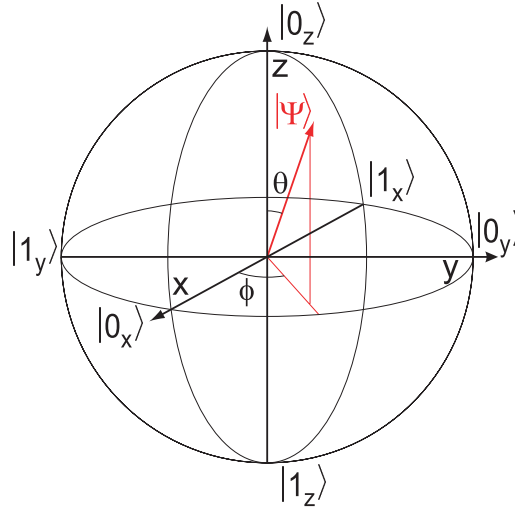


Figure 2.1: Representation of a general two-level state $|\Psi(\theta, \phi)\rangle$ as a vector on the Bloch sphere

2.1.2 Entanglement of two-qubit systems

In general a state of n qubits $|\Psi\rangle_{1\dots n}$ is called *entangled* if one cannot find a representation such that $|\Psi\rangle_{1\dots n}$ can be separated into a product state of the single qubits:

$$|\Psi\rangle_{1\dots n} \neq |\Psi\rangle_1 \otimes \dots \otimes |\Psi\rangle_n \quad (2.3)$$

However, if one can find such a representation the state is called *separable*. In a separable state measurement outcomes on one of the subsystems are totally independent of measurements on the other. This is not the case for entangled systems as can easily be seen at the example of the four Bell-states

$$|\Psi^-\rangle = \sqrt{\frac{1}{2}} (|0_z\rangle_1 |1_z\rangle_2 - |1_z\rangle_1 |0_z\rangle_2) \quad (2.4)$$

$$|\Psi^+\rangle = \sqrt{\frac{1}{2}} (|0_z\rangle_1 |1_z\rangle_2 + |1_z\rangle_1 |0_z\rangle_2) \quad (2.5)$$

$$|\Phi^-\rangle = \sqrt{\frac{1}{2}} (|0_z\rangle_1 |0_z\rangle_2 - |1_z\rangle_1 |1_z\rangle_2) \quad (2.6)$$

$$|\Phi^+\rangle = \sqrt{\frac{1}{2}} (|0_z\rangle_1 |0_z\rangle_2 + |1_z\rangle_1 |1_z\rangle_2) \quad (2.7)$$

which we here have written in the basis states of $\hat{\sigma}_z$. These states also form a complete set of eigenvectors for the two-qubit Hilbert-space.

Consider now, for example, the state $|\Psi^-\rangle$. If a projection measurement on particle 1 in the $\hat{\sigma}_z$ -basis yields the outcome “0”, then a subsequent measurement on

particle 2 in the same basis will always yield the outcome “1” and vice versa. So the measurement outcomes on such a Bell-state are always anti-correlated as long as one chooses the same measurement bases. However, these correlations entirely vanish if the measurements are performed in the bases of different Pauli operators.

Another interesting property of the Bell-states is that a measurement on only one of the particles always gives totally random outcomes. So no information can be gained about the state of the two-particle system by such a *local* measurement on only one qubit. In order to exactly identify a Bell-state, a state tomography of the entire 2-qubit system has to be performed that involves simultaneous measurements on the two particles in all three complementary bases [19].

Finally, the following two properties about entanglement should be mentioned [13]:

- Starting from a separable state, one can never create an entangled state only by *local transformations* on the single qubits. One always needs an interaction between the qubits (such as the spontaneous decay in our atom-photon entanglement scheme, see 2.2.1) or two particles that originate from a common source (such as the photons from a parametric down-conversion).
- A maximally entangled state stays maximally entangled under local unitary transformations of the subsystems since unitary transformations can always be reversed.

Such local unitary transformations are in our experiment for example given by the unwanted action of partially birefringent optical elements on the polarization state of the photon. Due to the invariance of entanglement against these transformations it is possible in the experiment to compensate these transformations without loss of the entanglement.

2.1.3 Fidelity

In order to determine the accuracy with which a desired state has been prepared in an experiment one needs a measure for the overlap between the desired and the prepared state. One way to do this is to calculate the *fidelity* F [20]. If the desired state is a pure state $|\Psi\rangle$, then the fidelity is:

$$F = \langle \Psi | \rho | \Psi \rangle \quad (2.8)$$

where ρ is the density matrix of the experimentally prepared state. For a perfect preparation of $|\Psi\rangle$ F equals one.

For determining ρ a full state tomography of the prepared state has to be performed. As stated above this requires measurements in all the complementary bases. An easier way to determine F is to suppose that the prepared state is in the state $|\Psi\rangle$ with a probability p and in the entirely mixed state with probability $(1 - p)$. Where the density operator of the entirely mixed state is $\frac{1}{4}\hat{\mathbb{1}}$. With this rather pessimistic assumption of white noise, ρ reads:

$$\rho = p \cdot |\Psi\rangle\langle\Psi| + \frac{(1 - p)}{4} \cdot \hat{\mathbb{1}} \quad (2.9)$$

The fidelity (2.8) can then be written as:

$$F = \frac{1 + 3p}{4} \quad (2.10)$$

If the desired state is a maximally entangled state, for example a Bell-state, then a criterion for deciding if the prepared state is entangled is given by [21]:

$$F > 0.5 \quad (2.11)$$

2.2 Atom-photon entanglement with ^{87}Rb

The aim of the present work is to create entanglement between a single ^{87}Rb atom and a single photon. As it was stated in the last section, an interaction between those particles is necessary in order to obtain an entangled state. This section describes the spontaneous decay process that leads to entanglement between the Zeeman state of the atom and the polarization state of the emitted photon. Moreover, a reference frame for our setup will be chosen in order to define the three complementary measurement bases for the photonic and the atomic qubit.

2.2.1 Creation of entanglement

For describing the process that yields the entangled atom-photon pair we consider the level scheme of ^{87}Rb depicted in figure 2.2. Shown are the two hyperfine levels $F = 1$ and $F = 2$ of the $5^2\text{S}_{1/2}$, $F = 1$ ground state as well as the hyperfine levels $F' = 0$ and $F' = 1$ of the $5^2\text{P}_{3/2}$ excited state.

For creating entanglement we now prepare the atom in the $F' = 0$ excited state. From there it can spontaneously decay via three decay channels into the three Zeeman-sublevels $m_F = \pm 1, 0$ of the $F = 1$ hyperfine ground state under the emission of a photon that can be σ^\pm or π -polarized. Here $m_F = \pm 1$ means that the atomic angular momentum is oriented parallel or anti-parallel to the quantization axis and $m_F = 0$ means that it is perpendicular to the quantization axis. In the case of the photon σ^\pm -polarization means that its spin is parallel or anti-parallel to the quantization axis and π -polarization means that it is perpendicular to the quantization axis. Due to conservation of angular momentum the polarization of the emitted photon depends on the Zeeman state the atom decays into (see figure 2.2).

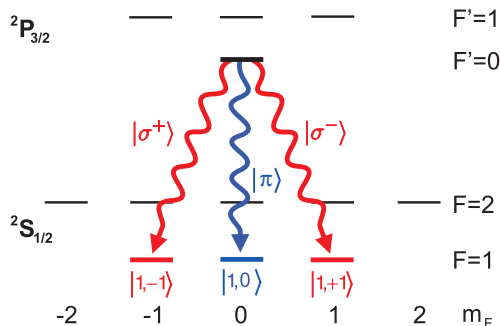


Figure 2.2: Scheme of the spontaneous decay leading to entanglement.

The relative amplitudes and phases between the decay channels are given by the Clebsch-Gordon coefficients of the respective transitions. In the present case they are the same for all of the three channels [22]. In the absence of external electric or

magnetic fields the three states into which the atom can decay are degenerate. Hence, the only possibility to distinguish the decay channels is given by the polarization of the photon and the Zeeman-state of the atom. Therefore the two-particle state after the decay can be written only in terms of the atomic Zeeman states and the photonic polarization states that result from the different decay channels:

$$|\Psi\rangle = \frac{1}{\sqrt{3}}(|\sigma^+\rangle|1, -1\rangle + |\pi\rangle|1, 0\rangle + |\sigma^-\rangle|1, +1\rangle) \quad (2.12)$$

This state is however only valid if one observes the emitted photon under the full solid angle of 4π around the atom. However, in our experiment we will use an objective with a certain optical axis and a single mode optical fiber behind it in order to collect the emitted photon. Therefore, we observe only along one distinct axis and the relative amplitudes in eq. (2.12) have to be weighted with the directional characteristic of the respective dipole transitions for σ^\pm and π light. Suppose the axis of the detection optics encloses an angle θ with the quantization axis. Then the dependence of the power P radiated into a solid angle Ω around this axis is given by [23]

$$\frac{dP_\pi}{d\Omega} = \frac{3}{8\pi} \sin^2 \theta \quad (2.13)$$

$$\frac{dP_\sigma}{d\Omega} = \frac{3}{16\pi} (1 + \cos^2 \theta) \quad (2.14)$$

for π - and σ -polarized, light respectively. Hence, if the collection optics is installed with the optical axis along the quantization axis (i.e. $\theta = 0$), the amplitude of π -light vanishes. As a result the state that is observed is the following Bell-state:

$$|\Psi^+\rangle = \frac{1}{\sqrt{2}}(|\sigma^+\rangle|1, -1\rangle + |\sigma^-\rangle|1, +1\rangle) \quad (2.15)$$

2.2.2 Definition of the measurement bases

When working with an entangled system of two physically different particles such as an atom and a photon, it is not always obvious in which measurement bases one will see the correlations mentioned in 2.1.2. It is therefore important to define in advance a reference frame for the setup and to identify the three complementary measurement bases for each of the particles.

We define the \vec{z} -axis to be along the quantization axis which in our case is determined by the optical axis of the microscope objective that collects the emitted photons (figure 2.3(a)). Then a measurement on the photonic qubit in the $\hat{\sigma}_z$ -basis is a projection onto the two circular polarization states $\{|\sigma^-\rangle, |\sigma^+\rangle\}$. The polarization states that are the eigenstates of $\hat{\sigma}_x$ and $\hat{\sigma}_y$ are now given by the decomposition of

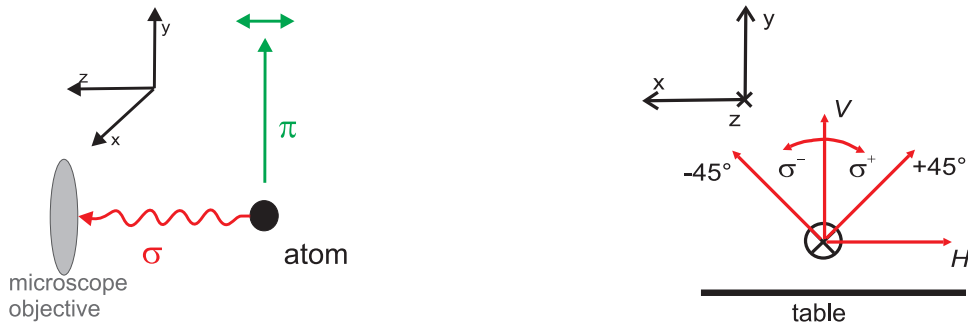


Figure 2.3: a) The quantization-axis \vec{z} is defined by the optical axis of the objective.
 b) Definition of polarizations for light traveling along \vec{z} .

the eigenstates of $\hat{\sigma}_x$ and $\hat{\sigma}_y$ in terms of the eigenstates of $\hat{\sigma}_z$ (see eq. (2.2)). They physically correspond to the linear polarizations $\{|H\rangle, |V\rangle\}$ and $\{|+45\rangle, |-45\rangle\}$, respectively [24]. The orientations of those polarizations with respect to the surface of the optical table and the quantization axis are defined as depicted in figure 2.3(b). In the case of the atom, a measurement in the $\hat{\sigma}_z$ -basis is a projection onto the Zeeman states $\{|1, -1\rangle, |1, +1\rangle\}$. Table 2.1 summarizes our choice of the measurement bases.

qubit	photonic state	atomic state
$ 0_x\rangle$	H	$\frac{1}{\sqrt{2}}(1, +1\rangle + 1, -1\rangle)$
$ 1_x\rangle$	V	$\frac{1}{\sqrt{2}}(1, +1\rangle - 1, -1\rangle)$
$ 0_y\rangle$	$+45$	$\frac{1}{\sqrt{2}}(1, +1\rangle + i 1, -1\rangle)$
$ 1_y\rangle$	-45	$\frac{1}{\sqrt{2}}(1, +1\rangle - i 1, -1\rangle)$
$ 0_z\rangle$	σ^+	$ 1, +1\rangle$
$ 1_z\rangle$	σ^-	$ 1, -1\rangle$

Table 2.1: Bases choice for the photonic and corresponding atomic state-readout

2.3 Entanglement of two remotely trapped atoms

The long term goal of our work is a system of two entangled atoms that are trapped at remote locations at a distance of 300 *m*. Such a configuration would e.g. allow a loophole-free test of Bell's inequality as will be outlined in chapter 2.4.

This section presents how entanglement can be established between trapped atoms at large distances by means of the so-called entanglement swapping protocol. After a general description of the protocol itself we address two-photon interference as the central part for realizing this protocol.

2.3.1 Entanglement swapping

The idea of entanglement swapping is to create entanglement between two particles at remote locations that have never interacted with each other [11]. The usual notation in quantum information science is to call the owners of those particles Alice and Bob. We denote Alice's and Bob's particles (in our case the atoms) 0 and 3, respectively (see Figure 2.4). Alice and Bob now entangle these primary particles with secondary particles 1 and 2 each (in our case this will be photons). Those secondary particles are then brought together and a Bell-state measurement on their shared two-particle state is performed (in our case on the polarization state of the photons, see 2.3.2). By quantum teleportation [11] this projection of the secondary particles onto an entangled state is then mapped onto the two-particle state of the primary particles.

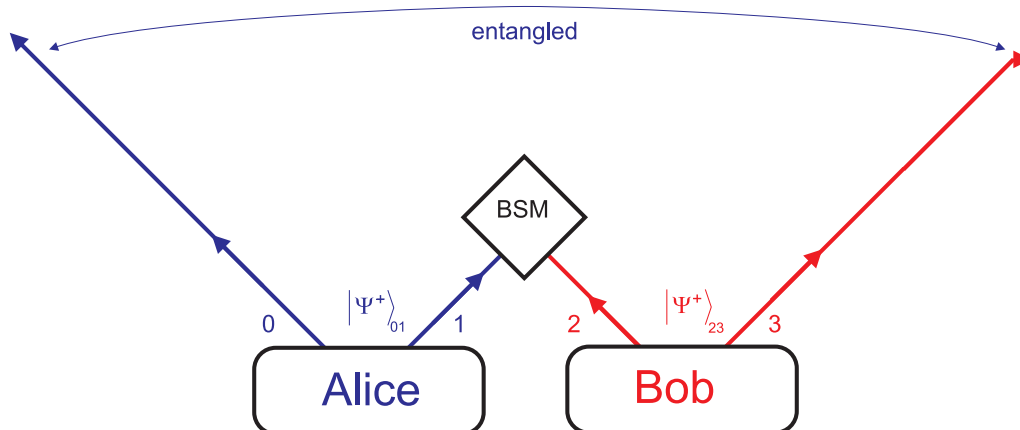


Figure 2.4: Scheme of entanglement swapping

This procedure can be described mathematically in the following way: After we have created an entangled atom-photon pair in the $|\Psi^+\rangle$ state (eq. 2.15), the total

four-particle state can be written in the form

$$|\Psi\rangle_{0123} = |\Psi^+\rangle_{01} \otimes |\Psi^+\rangle_{23} \quad (2.16)$$

Exploiting the completeness of the four Bell-states as a basis of a two-qubit Hilbert-space, the unity operator of the photon-subspace can be written in the form

$$\hat{\mathbb{1}}_{12} = |\Psi^-\rangle_{12} \langle\Psi^-|_{12} + |\Psi^+\rangle_{12} \langle\Psi^+|_{12} + |\Phi^-\rangle_{12} \langle\Phi^-|_{12} + |\Phi^+\rangle_{12} \langle\Phi^+|_{12} \quad (2.17)$$

Multiplication of the right side of (2.16) with this operator yields an expression for $|\Psi\rangle_{0123}$ in the basis of the Bell-states of the photons:

$$|\Psi\rangle_{0123} = \frac{1}{2} (|\Psi^+\rangle_{12} |\Psi^+\rangle_{03} - |\Psi^-\rangle_{12} |\Psi^-\rangle_{03} + |\Phi^+\rangle_{12} |\Phi^+\rangle_{03} - |\Phi^-\rangle_{12} |\Phi^-\rangle_{03}) \quad (2.18)$$

As one can see from this representation, a projection of the photons onto any of the Bell-states automatically projects the atoms onto the same Bell-state.

2.3.2 Two-photon interference

In our case the Bell-state measurement which is the central part of the entanglement swapping protocol shall be realized by interference of the photons on a beamsplitter. Depending on the two-photon polarization state the photons leave a beamsplitter either both on the same output port or one at each of the outputs. A projection onto the $|\Psi^-\rangle$ Bell-state can then be achieved by placing a single-photon detector behind each of the two output ports of the beamsplitter and registering *coincidence events* - i.e. events where one photon is detected at each detector [25, 26].

The characterizing parameter for the quality of the Bell-state measurement is the probability $p(|\Psi^-\rangle)$ of having projected onto the $|\Psi^-\rangle$ -state after a coincidence-detection. This probability decreases with the time delay between the detection of the two photons if the spectrum of the photons is incoherently broadened with respect to their natural linewidth [25, 26]. As a consequence only events with a certain detection time difference can be accepted for incoherently broadened photons and the rate of created entangled atom-atom pairs decreases.

In our case the photons that are created during the spontaneous decay of the atom are incoherently broadened due to two effects: First Doppler line broadening due to the thermal velocity distribution of the atom. And second broadening due to the thermal distribution of the potential energy of the atom in the trapping potential. This results in a distribution of the shift of the atomic ground state energy induced by the optical dipole laser (section 3.2). Thus the central frequency of the

transition of the spontaneous decay is thermally distributed as well. This effect is called *lightshift-broadening*. The temperature of the atom in the first trap setup was measured to be $T = 105 \mu\text{K}$ [27]. For this temperature the lightshift broadening causes a distribution of the transition frequencies of 4.4 MHz FWHM [27] whereas the width caused by Doppler broadening is of only 302 kHz.

For these incoherently broadened linewidths detailed calculations have been performed [26] in order to find the necessary detection time window. It was found to be 14 ns which is significantly shorter than the lifetime of the $5^2P_{3/2}$ excited state of 26 ns (and thus also shorter than the photon duration). Thus a large amount of the coincidence events would have to be rejected. Moreover, since our two dipole traps have different maximal trap depths, the central frequency of the photons emitted by the two traps is different. This latter effect would make it impossible to perform two-photon interference with our two trap setups.

A solution to this problem is to switch off the optical dipole trap during the time the atom is excited and emits the photon. In this case the photons will only be Doppler-broadened. Since this effect is one order of magnitude smaller than the lightshift broadening, the detection-time window can then be extended over the whole photon duration and no coincidence event has to be rejected. This method was examined for the first time in the course of the present work. The obtained results will be presented in section 3.7.

2.4 Tests of Bell's inequality

Despite the huge success of quantum mechanics in explaining a broad spectrum of physical phenomena from the microcosmos up to macroscopic objects of our everyday life there still remain questions about its conceptual foundations and interpretation.

First of all quantum mechanics only makes predictions about the outcome of measurements and only right after a measurement the real state of a system can be known with certainty according to this theory. It claims that a system has no definite *real* properties between measurements. Instead, the state of a system is described by a superposition of different possible states of which one is randomly chosen during the measurement process when the so-called collapse of the wavefunction takes place. Moreover, quantum mechanics doesn't seem to allow for a *local* description of the wavefunction collapse in the sense that it assumes an instantaneous collapse at any point of a spatially extended wavefunction during the measurement process.

This abandonment of the two fundamental ideas of *reality* and *locality* let Einstein, Podolsky and Rosen doubt that quantum mechanics is complete [1]. As an alternative local-hidden-variable (LHV) theories have been proposed that assume that physical systems carry additional parameters that are inaccessible by experi-

ment and that contain the information one would need to predict with certainty the outcome of any measurement.

Bell's inequality [3] gives an objective criterion that allows to decide whether such local hidden variables exist. It is an inequality for the outcomes of measurements on an entangled system of two spin- $\frac{1}{2}$ particles that always holds if LHVs exist, but is violated by quantum mechanical predictions. In the formulation of Clauser, Horne, Shimony and Holt this equation reads [28]:

$$S(a, a', b, b') := |E(a, b) - E(a, b')| + |E(a', b) + E(a', b')| \leq 2 \quad (2.19)$$

Where $E(a, b)$ is the expectation value for measurements on particle 1 under the angle a and particle 2 under the angle b . Quantum mechanics allows a maximal violation of eq. (2.19) with $S = 2\sqrt{2}$ for maximally entangled states for an appropriate choice of the measurement angles.

2.4.1 Loopholes

So far, all of the experiments that violated Bell's inequality left open at least one of the following loopholes, that still allow for the construction of local realistic theories:

- *Locality loophole:* The choice of the measurement basis of particle 1 and the end of the measurement on particle 2 and vice versa have to be *space-like separated* in order to exclude that the measurement outcome on either of the particles can be influenced by the measurement on the other via classical communication at the speed of light.
- *Detection loophole:* If it is not possible to read out the whole sample of entangled pairs due to a limited detection efficiency of the particles one is forced to make the *fair sampling assumption*. This presumes that the results obtained for the detected particles are representative for the whole sample. For an exclusion of LHV-theories a sufficiently high proportion of the entangled pairs have to be read out [29]. If the used entangled state is a $|\Psi^+\rangle$ -state this proportion is 83 %.

Up to now, it was possible to close the locality-loophole in experiments with entangled photons, that can easily be separated over large distances without loss of entanglement [8]. However, the limited efficiency of single photon detectors made it impossible to close the detection loophole¹. In contrary, experiments with entangled

¹Modern transition-edge superconducting (TES) photon detectors that show quantum efficiencies of 95% [30] might become an option in future.

trapped ions [9, 10] closed the detection loophole by exploiting the advantage that trapped massive particles can always be read out thus yielding an intrinsic detection efficiency of $\eta = 1$. In [10] entanglement between the ions was obtained by entanglement swapping via two-photon interference. However, the ions were only a few meters apart and thus the locality loophole could not be closed.

The aim of the present experiment is to exploit the advantages of photons and atoms. Recently, our group demonstrated that atom-photon entanglement can be distributed over long distances [15]. For this the photon was sent through a 300 m long optical fiber before the state readout was performed. It was shown that the entanglement can be maintained by appropriately stabilizing the fiber link. By using the entanglement swapping protocol it would thus be possible to create an entangled pair of ^{87}Rb atoms at distances that allow to close the locality loophole. Together with the high detection efficiency of the atoms a loophole-free Bell-test [31] seems feasible.

2.4.2 Technical requirements for a loophole-free Bell-test with two ^{87}Rb -atoms

So what are the technical requirements for a loophole-free test of Bell's inequality? First in order to close the locality loophole with two atoms at a distance of 300 m the choice of the measurement bases together with the measurements must be finished within $\frac{300\text{m}}{c} = 1\ \mu\text{s}$. This is not possible with our current atomic state detection, but will become feasible by the implementation of a faster detection scheme based on state-selective ionization and subsequent detection of the ionization fragments [31].

Second for a clear violation of Bell's inequality by three standard deviations we estimate to need about 3470 events [31]. Given a conservatively estimated event rate of successful entanglement swapping of approximately one per 5 minutes we obtain a total measurement time of about 12 days. The event rate directly depends on the following three parameters:

1. loading-rate and lifetime of atoms in the trap
2. repetition rate of the atom-photon entanglement process
3. collection efficiency of the emitted photons

The loading rate and lifetime of the atoms have already been optimized for both trap setups and in the second trap setup an objective with a higher numerical aperture of $NA = 0.5$ has been installed for increasing the collection efficiency of the spontaneously emitted photons [18]. In the course of the present work the repetition rate of created atom-photon pairs was partially optimized by reducing the duration of the optical pumping process of the atomic state preparation (see section 3.6).

And third the photons used for the two-photon interference must be spectrally indistinguishable. This becomes possible by switching off the dipole trap during the excitation and photon emission process. This method was also examined during this work (see section 3.7).

3 Experimental realization of atom-photon entanglement

Atom-photon entanglement is the key technology for being able to perform the entanglement swapping protocol that shall yield the entangled atom-atom pair described in section 2.3. Such a hybrid entangled system consisting of particles of different species was first realized in 2004 using $^{111}\text{Cd}^+$ -ions stored in a single ion trap [32]. In our experiment atom-photon entanglement is created in the spontaneous decay of a single neutral ^{87}Rb -atom that is stored in an optical dipole trap. The decay produces a photon of which the polarization state is entangled with the Zeeman state of the atom. Various laser techniques are necessary for trapping the single atom, for the preparation of the excited state as well as the readout of the atomic state. Moreover, it has to be assured that the atomic qubit is sufficiently stable during the time that passes between the creation of the entangled state. These experimental steps are going to be presented in the following. At the end of this chapter, measurements will be presented that show that the prepared atom-photon state is entangled.

3.1 Technical components

This section briefly presents the technical components necessary for performing the envisaged experiment:

3.1.1 Laser system

Elaborate laser techniques are used in this experiment for performing manipulations on the Zeeman- and hyperfine-levels of the atom such as laser cooling, optical dark state pumping and a coherent Zeeman state-selective transfer between two hyperfine levels. For this purpose the lasers have to spectrally resolve different atomic hyperfine transitions that are separated by only 72 MHz (figure 3.1). A convenient method in atom physics to achieve such high precision is to use grating-stabilized diode lasers of which the frequency is stabilized to the optical transitions of the desired atomic species by means of Doppler-free saturation spectroscopy [33].

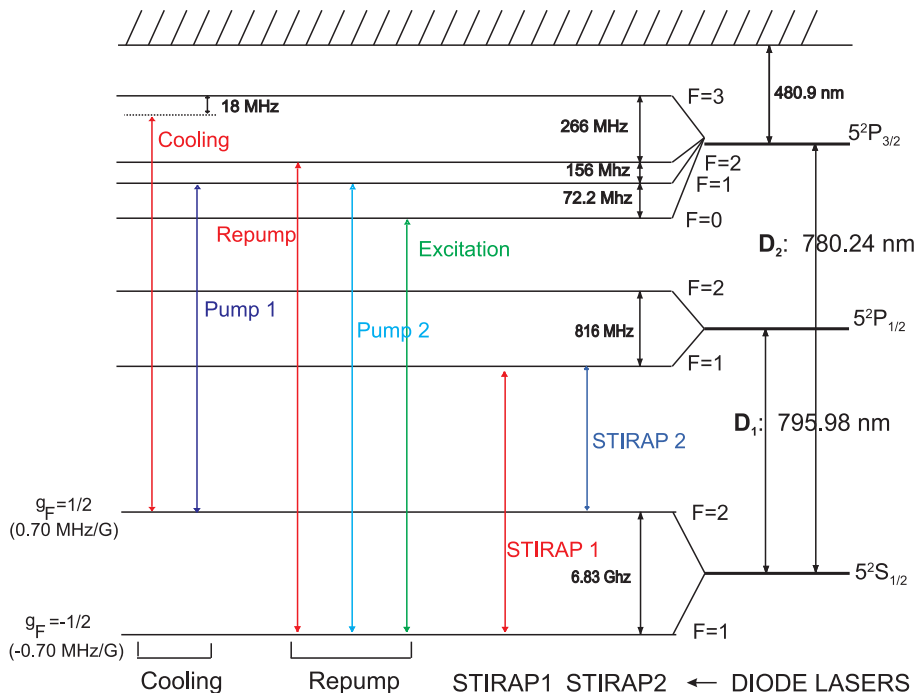


Figure 3.1: Level scheme of ^{87}Rb and the transitions that can be addressed by shifting the frequency of the four diode lasers with AOMs.

In our setup we have four such diode lasers - two for the D₁-line of ^{87}Rb and two for the D₂-line (see figure 3.1). The large energy-separation between the $|F = 1\rangle$ and $|F = 2\rangle$ ground-states of 6.8 GHz and between the $^2P_{1/2}$ and $^2P_{3/2}$ excited states requires separate diode lasers for each of the four possible transitions. The spectral linewidth of the created laser beams is about 0.6 MHz . Distinct hyperfine levels within the excited states can be addressed by shifting the frequency of the respective laser with acousto-optical modulators (AOM) by up to $\pm 200\text{ MHz}$. The AOMs are also used to switch the laser beams on and off with rise and fall times of $\sim 10 - 20\text{ ns}$. Finally, a fifth diode laser without frequency stabilization is used to produce the light for the optical dipole trap at 856 nm .

After having passed the AOMs the light is coupled into single-mode optical fibers and guided them to the atom trap. The fibers also serve as spatial mode filters such that the beams get a clean Gaussian profile which simplifies their further manipulation.

3.1.2 Pattern generator

For creating laser pulse sequences on the timescale of the atomic decay time (26 ns) we use an electronic pattern generator [34] whose output signals are used

to switch the drivers of the AOMs. 16 different pulse patterns for controlling 48 devices simultaneously with a selectable time resolution of optionally 20 ns or 2 μ s can be loaded into the device. Different phases of the experiment such as loading of the single atom trap, optical pumping and excitation or atomic state readout are each programmed in a separate pattern. Real-time switching between the patterns by external signals then allows to react on events like an atom entering the trap, detection of a single photon etc.

3.1.3 Recording of events

For detection of single photons emitted by the atom we use two actively quenched avalanche photo-diodes (APD) with a dark count rate of $\sim 70 \frac{\text{counts}}{\text{s}}$ and a quantum efficiency of 0.6. Event-signals from the APDs are read in by two channels of a timestamp unit, that tags them with the specific APD-number and a timestamp with a resolution of 125 ps. Two further channels of the timestamp device are used to record trigger pulses from the pattern generator. These trigger pulses are generated to mark the beginning of different experimental phases like excitation of the atom or the atomic state readout process. Such marks are necessary for the interpretation of the photon signals during the evaluation of the experimental runs.

3.2 Single atom trap

For performing the experiment of atom-photon entanglement one first has to prepare a single atom at a fixed position and well isolated from interactions with the environment. For this a single-atom trap has been set up [16, 18]. In the following the three major building blocks that are needed for such a trap will be explained.

3.2.1 Vacuum system

The single atom trap is created in the center of a spectroscopic glass cell (figure 3.2) that allows good optical access to the trap from all spatial directions. This glass cell is attached to an ultra-high vacuum system. A Rubidium dispenser driven at a current of $\sim 5 - 6$ A constantly evaporates a mixture of ^{87}Rb and ^{85}Rb atoms into the vacuum chamber. At the same time an ion getter pump permanently absorbs atoms of all species from the gas within the chamber. These two components create an equilibrium state in which the major proportion of the gas in the glass cell is made up of Rubidium atoms at a pressure of $10^{-9} - 10^{-10}$ mbar. Such a low pressure is necessary in order to reduce the mean time between two subsequent collisions of an atom with other atoms from the gas. This is vital for a long lifetime of the single atom in the trap.

3.2.2 Magneto-optical trap

The single-atom dipole trap described below provides only a conservative trapping potential that is much shallower than the mean-kinetic energy of atoms in a gas at room temperature. In order to load atoms into this trap one must thus first create an ensemble of atoms with an energy well below the depth of the dipole trap. This is achieved by the means of a magneto-optical trap (MOT) [35]:

It basically consists of three pairs of circularly polarized counterpropagating laser-beams - one along each of the spatial axes - that intersect at the position of the optical dipole trap (figure 3.2). The frequency of those beams is red-detuned by 18 MHz with respect to the atomic $5^2S_{\frac{1}{2}} |F = 2\rangle \rightarrow 5^2P_{\frac{3}{2}} |F' = 3\rangle$ transition of ^{87}Rb (see the level scheme in fig. 3.4). As a consequence, Doppler-cooling effects occur when a ^{87}Rb -atom moves along any direction of the beams. This creates a dissipative force field that is made position-dependent by the application of a three-dimensional magnetic quadrupole-field in such a way that atoms crossing the intersection region of the beams are slowed down and driven backwards to the trap center when they try to leave it. The result is a cloud of cold ^{87}Rb -atoms with a size of about 1 mm at the crossing of the cooling beams.

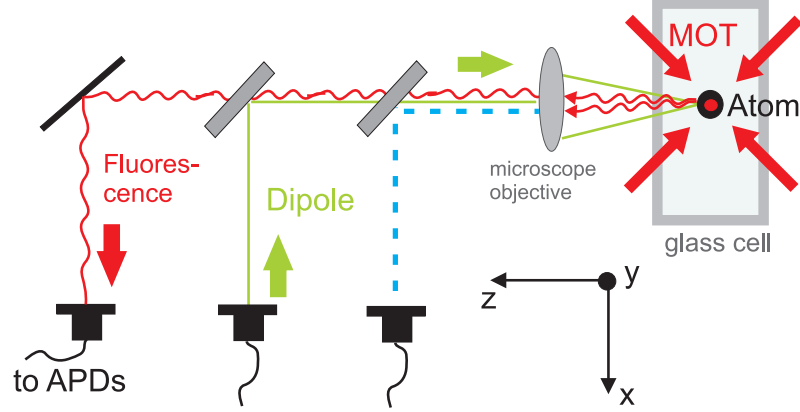


Figure 3.2: Trap setup: The magneto-optical trap (MOT) is created by three pairs of counterpropagating beams. The center of the MOT is overlapped with the focus of the beam that creates the optical dipole trap. Dipole trap and fluorescence detection are in a confocal configuration. Their optical paths are overlapped by a dichroic mirror. The blue dashed line indicates the beam of the ionization laser for the fast atomic state readout (not yet implemented).

The temperature of the atoms in this cloud can be considered to be on the order of the Doppler-temperature $T_{dop} = 146 \mu\text{K}$ [22]. However, since the cooling beams are circularly polarized, sub-Doppler cooling effects also occur so that even temperatures below the Doppler-limit are possible [36, 35].

During the cooling process atoms can off-resonantly decay from $F' = 3$ to the $F = 1$ ground state where they are no more resonant to the cooling light. In order to recycle them a repump laser that is resonant to the $S_{\frac{1}{2}} |F = 1\rangle \rightarrow P_{\frac{3}{2}} |F' = 2\rangle$ transition pumps them back into $F = 2$.

3.2.3 Optical dipole trap

The principle of an ODT is based on the AC-Stark effect that induces a shift of the energy levels of an atom in a light-field that is far detuned from an atomic resonance. By this an atom in this light field obtains a potential energy U that is equal to the energy shift of its ground state. For Alkali atoms such as our ^{87}Rb a red detuning leads to a lowering of the ground state energies. The relation between the intensity $I(\vec{r})$ of the light field and the resulting energy shift $U(\vec{r})$ of the atomic ground state is given by [37]:

$$U_{dip}(\vec{r}) = \frac{\pi c^2 \Gamma}{2\omega_0^3} \left(\frac{2 + P g_F m_F}{\Delta_{2,F}} + \frac{1 - P g_F m_F}{\Delta_{1,F}} \right) I(\vec{r}) \quad (3.1)$$

Here g_F is the Landé factor of the respective hyperfine level F and Γ and ω_0 are the decay rate and transition frequency of the D_1 -line, respectively. $\Delta_{1,F}$ and $\Delta_{2,F}$ are the detunings of the light field with respect to the transition frequencies between the hyperfine ground state F and the $^2P_{1/2}$ and $^2P_{3/2}$ excited state. P finally equals 0 and ± 1 for linear and σ^\pm polarized light.

If the light field is created by a Gaussian laser beam, then the atom is attracted to its focus where the intensity is the highest and the lowering of the ground state energy is maximal. So a far red-detuned Gaussian beam can serve as a trap for neutral ^{87}Rb atoms. In our case we use the Gaussian beam of a diode laser with a wavelength of $\lambda = 856 \text{ nm}$. This wavelength is far red-detuned compared to the D_1 - and D_2 -lines of ^{87}Rb (795 nm and 780 nm, respectively). The beam of vertical linear polarized light is focused down to a waist of $w_0 = 1.9 \mu\text{m}$ [18] which results in a Rayleigh length of $z_R = 13.25 \mu\text{m}$. For a laser power of 15 mW the maximal trap depth given by the energy shift at the focus of the beam then is:

$$U_0 = 1.5 \text{ mK} \quad (3.2)$$

It has been verified that for the chosen waist and trap depth a blockade effect ensures that not more than one atom can remain in the trapping potential simultaneously [18].

The mean lightshift induced by the dipole laser increases the central transition frequencies of the D_1 - and D_2 -lines of the trapped atom by $\sim 28 \text{ MHz}$. The potential of the trap can be considered approximately harmonic and the oscillation frequencies in the radial mode (perpendicular to beam axis) and the longitudinal mode (parallel to beam axis) are:

$$\omega_r = \sqrt{\frac{4U_0}{m w_0^2}} = 2\pi \cdot 63,5 \text{ kHz} \quad (3.3)$$

$$\omega_l = \sqrt{\frac{2U_0}{m z_R^2}} = 2\pi \cdot 6,37 \text{ kHz} \quad (3.4)$$

Such an optical dipole trap is the best suited instrument for our purpose. The energy shift between different Zeeman levels is zero for linearly polarized light and due to the far detuning the scattering rate of the trapping light by the atom is negligibly small. These advantages allow for the control and storage of an atom in a coherent superposition state of Zeeman levels for sufficiently long times.

Fuorescence detection and loading of the ODT

Figure 3.2 shows the whole trap setup. The ODT-beam is focused down to the center of the glass cell by a microscope objective with an effective focal length f_{eff} of 13 mm and a numerical aperture of 0.5. such that the focus overlaps with the MOT-cloud. The same objective is used to collect fluorescence photons from the atom. Those are coupled into a single-mode optical fiber that guides them to the

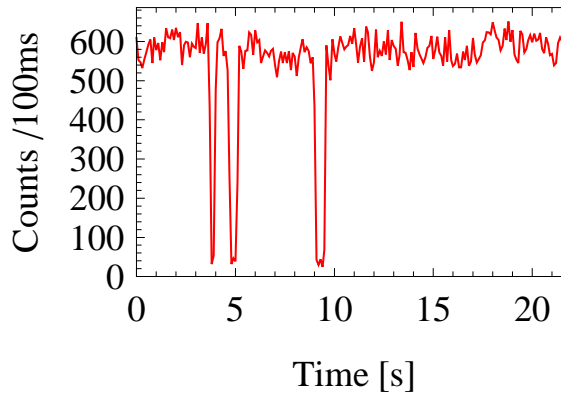


Figure 3.3: Fluorescence signal at the APDs when atoms enter and leave the trap.

APDs. A cold atom from the MOT that crosses the trapping potential of the ODT is further cooled during that time due to ongoing scattering of cooling light. If it thereby loses enough energy such that its total energy is less than the depth U_0 of the ODT, it will stay trapped there. As a consequence the count rate at the APDs rises abruptly due to the fluorescence induced by the cooling beams (figure 3.2.3). When it exceeds a predefined value, the magnetic field of the MOT is switched off so that the cloud of cold atoms disperses and a single atom remains inside the ODT. For a more detailed description of the physics of the loading process see [18]. Due to the red detuning of the cooling beams the atom is not heated while scattering light from them but rather continues to be cooled. This provides the possibility to survey the presence of the atom in the trap by detection of its fluorescence over long periods of time (several seconds).

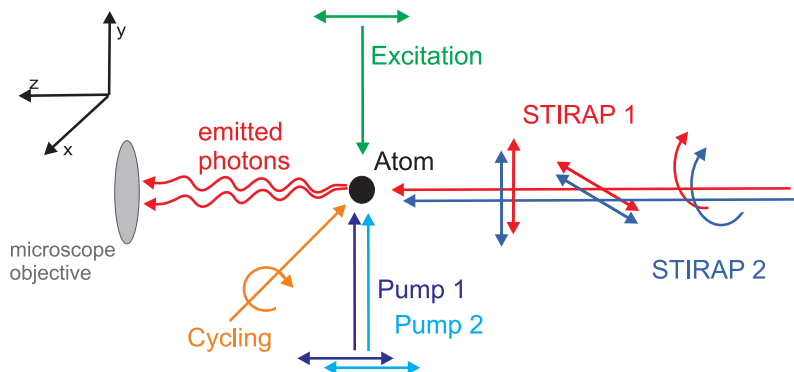


Figure 3.4: Sketch of the geometrical alignment and the polarizations of the lasers that are used to generate and verify atom-photon entanglement. The quantization axis \hat{z} is defined by the optical axis of the microscope objective that collects the spontaneously emitted photons. For clarity, the MOT- and ODT-beams are not shown here.

3.3 Overview of the experimental procedure

The experimental procedure for creating and verifying atom-photon entanglement with a single ^{87}Rb -atom consists of the following steps:

1. Optical pumping into the initial ground state $|F = 1, m_F = 0\rangle$
2. From there, excitation to $|F' = 0, m'_F = 0\rangle$ in $^2P_{3/2}$ and collection of the photon that is emitted in the subsequent sponaneous decay
3. Projection measurement on the polarization state of the photon
4. Conditioned upon the detection of a photon, perform the atomic state-readout

These steps shall now be presented in more detail.

1. **Optical pumping** In order to allow for a high efficiency of the excitation process, the first step is to optically pump the atom into the desired $|F = 1, m_F = 0\rangle$ -state. For this purpose two continuous π -polarized laser-beams are applied simultaneously (see figures 3.4 and 3.5(a)): Pump1 that is resonant to the $|F = 2\rangle \rightarrow |F' = 1\rangle$ transition of the D_2 -line and Pump2 that is resonant to $|F = 1\rangle \rightarrow |F' = 1\rangle$. Additionally, the cooling beams of the magneto-optical trap are switched on that couple to the $m'_F = \pm 2$ sublevels of the $F = 2$ hyperfine state. The atom continuously scatters light from those lasers until it decays into the $|F = 1, m_F = 0\rangle$ -state. In this state the atom is no more resonant to any of the applied lasers since the transition $|F = 1, m_F = 0\rangle \rightarrow |F' = 1, m'_F = 0\rangle$ is forbidden by the selection rules for dipole transitions.

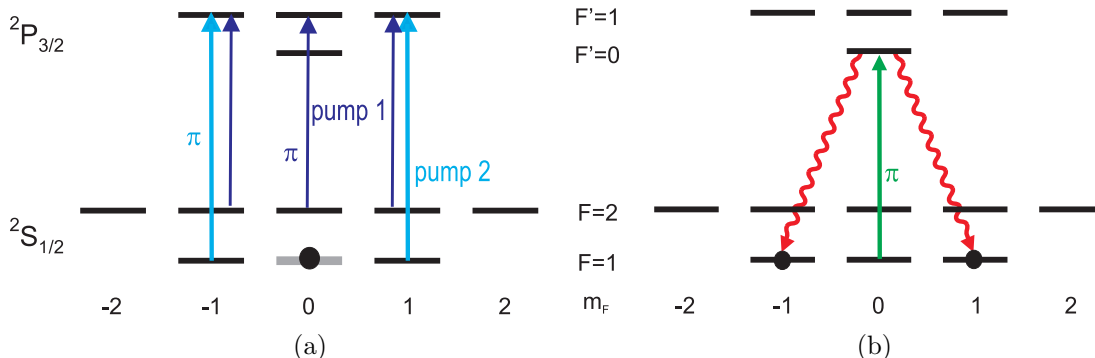


Figure 3.5: a) Optical pumping into the atomic dark state $|F = 1, m_F = 0\rangle$. Additional cooling-light for emptying $|F = 2, m_F = \pm 2\rangle$ is not shown here. b) Excitation to $|F' = 0, m'_F = 0\rangle$ and subsequent decay to $|F = 1\rangle$ that produces the entangled atom-photon pair.

2. **Excitation and spontaneous decay** The next step is to excite the atom to ${}^2P_{3/2} |F' = 0, m'_F = 0\rangle$. This is done by a short π -polarized light pulse as depicted in figure 3.5(b). As explained in section 2.2.1 the subsequent spontaneous decay yields a photon whose polarization-state is entangled with the Zeeman-state of the atom. This photon is collected by a microscope objective (figure 3.4) and coupled into a single-mode optical fiber that guides it to the photonic state analyzer.
3. **Analysis of the photonic state** The projection measurement of the photonic polarization state is accomplished by sending the photon onto a polarizing beam splitter (PBS) and detecting the photon with single-photon detectors (APD) placed behind the output ports of the PBS (figure 3.6(a)). By rotating a $\lambda/2$ - and a $\lambda/4$ -waveplate that are installed in front of the PBS one can select any measurement basis on the Bloch-sphere. A detection of the photon at one of the APDs now projects the atom onto the corresponding superposition of Zeeman-sublevels as given in table (2.1).
4. **Readout of the atomic state** The detection of the atomic Zeeman-state consists of two steps as depicted in figure 3.6(b): First the superposition of the two Zeeman-states $|1, -1\rangle$ and $|1, +1\rangle$ is mapped onto a superposition of the hyperfine-levels $|F = 1\rangle$ and $|F = 2\rangle$ by means of a so called STIRAP-technique. Subsequently a push-out pulse is applied that removes the atom from the trap if it is in the $F = 2$ hyperfine state. The original Zeeman state can then be determined by verifying whether the atom is still present in the trap after the push-out pulse. A detailed description of this readout scheme is given in the following section.

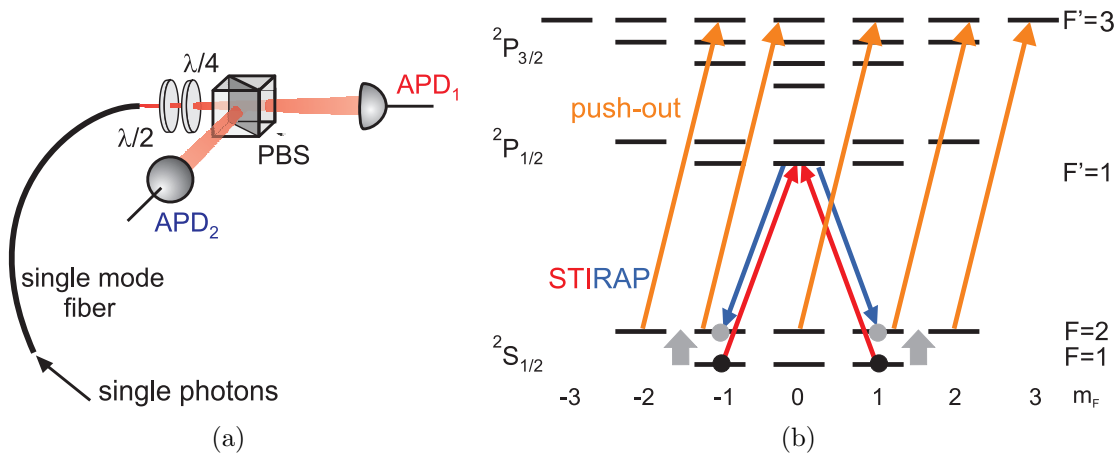


Figure 3.6: a) Setup for the measurement of the photonic polarization state. b) Atomic state-readout: The STIRAP pulse state-dependently transfers the atom to $|F = 2\rangle$ from where it is heated out of the trap by resonantly scattering light from the push-out laser.

In the experiment not every pump-excitation process is followed by the detection of a photon. Several effects lower the efficiency of this process: First, the optical pumping does not lead to a perfect occupation of the $|1, 0\rangle$ ground-state. Moreover, not every excitation pulse leads to the emission of a photon and only a small fraction of the photons is detected due to the limited numerical aperture of the microscope objective, coupling losses into the single-mode fiber and the limited detection efficiency of the APDs. The overall *excitation efficiency* - i.e. the probability to detect a photon at one of the APDs after an excitation pulse - is about 2.2%. Hence, the pumping-excitation process is repeated many times and the atomic state readout is only performed conditioned upon the detection of a photon. After every 10th pump-excitation cycle the atom has to be cooled again for $400 \mu\text{s}$ in order to compensate the heating induced by the pumping and excitation processes.

3.4 Readout of the atomic state

For verifying entanglement between the atom and the photon one must be able to perform a projection measurement on the atomic qubit that is encoded in a superposition of the $m_F = \pm 1$ Zeeman sublevels of the $F = 1$ hyperfine ground state. In our experiment this is done in a two-step process: First a certain superposition of the Zeeman sublevels is transferred to the $|F = 2\rangle$ hyperfine ground state while the orthogonal superposition stays in $F = 1$. Then a projection measurement onto the two hyperfine levels is performed.

This section begins with a paragraph on the hyperfine state readout. Thereafter a theoretical description of the STIRAP (*stimulated Raman adiabatic passage*) is given for a simple three-level system. In a second step it will be explained how this process can be made sensitive to different superpositions of Zeeman states. In the end the setup for its experimental realization is presented together with measurement results of the accuracy of the state detection.

3.4.1 Hyperfine state detection

Our hyperfine state detection works by state dependently removing the atom from the trap. This is realized by a $12\ \mu\text{s}$ long laser pulse that is tuned to the $S_{1/2}, F = 2 \rightarrow P_{3/2}, F' = 3$ transition (see figure 3.6(b)). This laser is σ^+ -polarized so that the atom is optically pumped to the $m_F = 3$ Zeeman level of the $F = 2$ ground state within several scattering processes. After it has arrived there, it continuously scatters light on the closed transition between the $F = 2, m_F = 3$ ground- and $F' = 3, m'_F = 4$ excited state until the accumulated photon recoil pushes it out of the trapping potential. The big separation of 6.8 GHz between the two hyperfine ground states strongly suppresses off-resonant scattering if the atom is in $|F = 1\rangle$. So in this case the atom stays in the trap. The hyperfine state can then be determined by verifying the presence of the atom in the trap after the push-out process. This is done by switching on the cooling and repump light of the magneto-optical trap and counting fluorescence photons from the atom for 10 ms.

The accuracy of identifying the states correctly is given by the probabilities, that an atom in $|F = 1\rangle$ is redetected after the push-out process and that an atom in $|F = 2\rangle$ is not. The measured accuracies are [17]

$$\begin{aligned} |F = 1\rangle: & \quad 98.3 \pm 1.3\% \\ |F = 2\rangle: & \quad 97.1 \pm 0.3\% \end{aligned} \tag{3.5}$$

The efficiency of the push-out process is mainly limited due to polarization errors of the cycling laser. By this the atom may leave the closed transition and off-resonant decay into $F = 1$ can take place from where the atom is no more resonant to the cycling laser. The limited probability to redetect the atom if it was in $F = 1$ is due

to collisions with atoms from the background gas that remove the atom from the trap during the relatively long fluorescence detection phase.

3.4.2 STIRAP for a three-level system

The task of the STIRAP-process is to transfer the atom from $F = 1$ to $F = 2$ depending on its Zeeman state. In this section we first describe the physics of the transfer itself. Afterwards it will be explained how this transfer can be made sensitive to a certain superposition of Zeeman states.

We consider the case of a three-level system with the two ground states $|F = 1\rangle$ and $|F = 2\rangle$ and the $|F' = 1\rangle$ hyperfine level of the ${}^2P_{1/2}$ excited state as depicted in figure 3.7(a). We now couple each of the ground states to the excited state by two light fields with Rabi-frequencies Ω_1 and Ω_2 . The Hamiltonian for the interaction of the atom with this light-field in the basis of the three atomic eigenstates $\{|F = 1\rangle, |F = 2\rangle, |F' = 1\rangle\}$ then reads:

$$\hat{H}_{int} = \frac{\hbar}{2} \begin{pmatrix} 0 & 0 & \Omega_1 \\ 0 & 0 & e^{i\delta}\Omega_2 \\ \Omega_1 & e^{-i\delta}\Omega_2 & 0 \end{pmatrix} \quad (3.6)$$

where δ is the relative phase between the two laser-fields. By calculating the eigenstates of the total Hamiltonian $\hat{H}_{atom} + \hat{H}_{int}$ for a given configuration of light fields Ω_1 and Ω_2 one obtains the following result. One of the eigenstates is given by:

$$|\Psi_0\rangle = \frac{1}{\sqrt{\Omega_1^2 + \Omega_2^2}} (\Omega_2 |F = 1\rangle - e^{i\delta}\Omega_1 |F = 2\rangle) \quad (3.7)$$

First of all, this state has the property that it contains no contribution from the excited state $|F' = 1\rangle$ which means that the excited state is not populated. Thus it can be excluded that spontaneous decay happens if the atom is in this eigenstate of the Hamiltonian. Secondly, the ratio between the populations in the two ground states depends on the ratio between Ω_1 and Ω_2 - i.e. the ratio of the two field intensities. By introducing the angle φ via

$$\tan \varphi = \frac{\Omega_1}{\Omega_2} \quad (3.8)$$

the state $|\Psi_0\rangle$ can be written as:

$$|\Psi_0\rangle = \cos \varphi |F = 1\rangle - e^{i\delta} \sin \varphi |F = 2\rangle \quad (3.9)$$

Suppose now that the atom is initially in the $|F = 1\rangle$ hyperfine level. A coherent transfer of the population from $|F = 1\rangle$ into $|F = 2\rangle$ can then be performed by

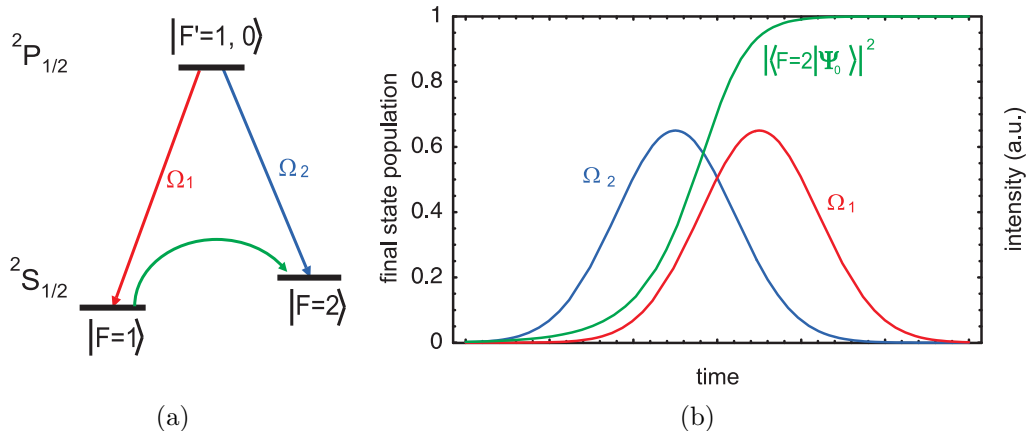


Figure 3.7: STIRAP in a three level system: a) Light fields Ω_1 and Ω_2 couple the initially populated state $|F = 1\rangle$ and the desired final state $|F = 2\rangle$ to the excited level $|F' = 1\rangle$. b) Temporal shape of the light pulses and resulting evolution of the population in $|F = 2\rangle$ (green line).

applying the pulse sequence depicted by the red and blue curves in figure 3.7(b): Starting with both fields off one first creates a field configuration such that the atomic eigenstate $|F = 1\rangle$ is identical to the eigenstate $|\Psi_0\rangle$ of H_{int} (i.e. $\varphi = 0$). This is achieved by setting $\Omega_2 \gg \Omega_1$. Then Ω_1 is switched on as well and the ratio between the field intensities is adiabatically inverted until $\Omega_2 \ll \Omega_1$. In this field configuration the eigenstate $|\Psi_0\rangle$ equals $|F = 2\rangle$. The field Ω_1 can then be turned off and the transfer of the whole population to the desired $|F = 2\rangle$ -state is completed. The temporal evolution of the population in $|F = 2\rangle$ during this process can be seen from the green curve.

This population transfer is based on the adiabatic theorem of quantum mechanics which states that a system that is initially in an eigenstate of its Hamiltonian stays in this eigenstate under *adiabatic* variation of the Hamiltonian - in our case the light intensities. The criterion for adiabaticity of the STIRAP process can be expressed by [38]

$$\sqrt{\Omega_1^2 + \Omega_2^2} \cdot \frac{1}{\dot{\varphi}} \gg 1 \quad (3.10)$$

This means that the faster the pulses are varied, the higher must be the field intensities. If this criterion is not fulfilled, the atomic state cannot follow the field variation. It partially leaves the eigenstate $|\Psi_0\rangle$ and as a result the efficiency of this process is reduced. Additionally, the phase δ in (3.7) has to be constant in order to guarantee the adiabaticity of the transfer [18]. For this the two laser fields must have a fixed phase relation. If these conditions are ideally fulfilled the STIRAP process allows for a transfer efficiency of one.

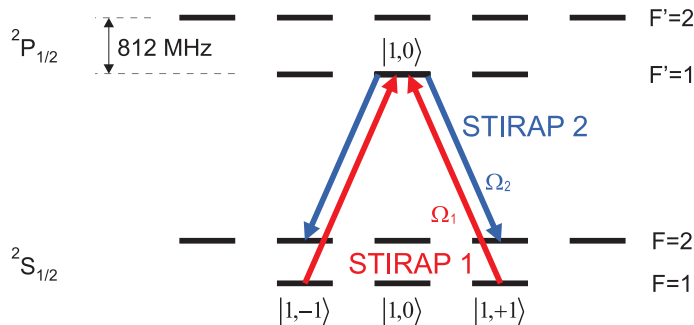


Figure 3.8: Zeeman state-selective STIRAP: The light fields Ω_1 , Ω_2 can be decomposed into a superposition of σ^+ and σ^- . A certain superposition of $|1, -1\rangle$ and $|1, +1\rangle$ then is dark to the STIRAP1 laser field.

3.4.3 Zeeman state-selective STIRAP

In our experiment the STIRAP-transfer shall only take place for a certain superposition of the $|1, \pm 1\rangle$ sublevels of $|F = 1\rangle$ while leaving the orthogonal superposition unaffected. The question which superposition is transferred is decided by the polarization of the STIRAP1 laser. Let us write the polarization state of the STIRAP1 laser as a superposition of σ^+ and σ^- polarization as depicted in figure 3.8

$$|\mathbf{P}\rangle = \cos \frac{\theta}{2} |\sigma^+\rangle + e^{i\phi} \sin \frac{\theta}{2} |\sigma^-\rangle \quad (3.11)$$

As can be shown [39, 35], there is a coherent superposition of Zeeman levels in which the atom does not couple to a STIRAP1 laser with the above polarization (such a state is called a *coherent dark state*). This superposition is:

$$|\Psi_D\rangle = \cos \frac{\theta}{2} |1, +1\rangle + e^{i\phi} \sin \frac{\theta}{2} |1, -1\rangle \quad (3.12)$$

where the index D stands for “dark“ state. In contrast, the superposition orthogonal to (3.12) is a “bright” state to STIRAP1 and is entirely transferred.

One must add here that populations in $|1, 0\rangle$ are transferred for any STIRAP polarization. For the interpretation of the entire readout sequence of STIRAP and subsequent hyperfine state detection this means the following: If the atom is redetected after the hyperfine state detection, one can say with certainty that a projection onto the dark state $|\Psi_D\rangle$ has taken place. If it is not redetected, the atom either was in the bright state *or* in $|1, 0\rangle$. This will become important when discussing the results of the Larmor precession measurements in section 3.5 where rotation of the atomic spin out of the qubit-subspace $\{|1, -1\rangle, |1, 1\rangle\}$ into the $|1, 0\rangle$ -state becomes possible.

Suppression of off-resonant transfer via $|F' = 2\rangle$

Up to now the polarization of STIRAP2 did not play a role for the Zeeman state-selectivity of the transfer process. However, for the high intensities we need in order to fulfill the adiabaticity criterion (3.10) off-resonant coupling to the excited hyperfine level $|F' = 2\rangle$ occurs. In this case transitions become possible to which the originally dark state $|\Psi_D\rangle$ is bright. A transfer can then still be suppressed by an appropriate choice of the polarization of Ω_2 [27]. For a polarization of STIRAP1 given by eq. (3.11) the polarization of STIRAP2 has to be:

$$|\mathbf{P}\rangle = \sin\frac{\theta}{2} |\sigma^+\rangle + e^{i\phi} \cos\frac{\theta}{2} |\sigma^-\rangle \quad (3.13)$$

So for linear polarization ($\theta = \pi/2$) the two STIRAP fields need to have parallel polarization, and for circular polarization ($\theta = 0, \pi$) they need to be orthogonally polarized.

Summing up one obtains the following table for the relations between a desired dark state and the necessary STIRAP polarizations:

atomic dark state	STIRAP1	STIRAP2
$\frac{1}{\sqrt{2}}(1, +1\rangle + 1, -1\rangle)$	H	H
$\frac{1}{\sqrt{2}}(1, +1\rangle - 1, -1\rangle)$	V	V
$\frac{1}{\sqrt{2}}(1, +1\rangle + i 1, -1\rangle)$	+45	+45
$\frac{1}{\sqrt{2}}(1, +1\rangle - i 1, -1\rangle)$	-45	-45
$ 1, +1\rangle$	σ^+	σ^-
$ 1, -1\rangle$	σ^-	σ^+

3.4.4 Experimental realization of STIRAP

For the creation of the STIRAP pulses Ω_1 and Ω_2 we use light from two separate diode lasers, each of which is stabilized to the corresponding transition. The relative time delay between the pulses as well as their duration can be adjusted by electronic delay circuits. The rising and falling edges of the pulses created by the pattern generator would be too steep to fulfill the adiabaticity criterion. In order to smoothen them, low-pass filters with a cut-off frequency of 14 MHz are inserted at the inputs of the AOM-drivers.

Another condition for an adiabatic transfer is that the phase stability between the two lasers STIRAP1 and 2 must be guaranteed. Their phase fluctuation $\frac{d\delta}{dt}$ has been measured to be about $2\pi \cdot 170$ kHz [18], so over a time of $\frac{1}{170 \text{ kHz}} = 5.9 \mu\text{s}$ the phase turns by 2π . The transfer then has to be finished in a considerably shorter time. This limits the duration of the pulses and thus gives a lower bound for the speed of the field variation $\dot{\varphi}$. Figure 3.9 shows a plot of the pulse sequence we use measured

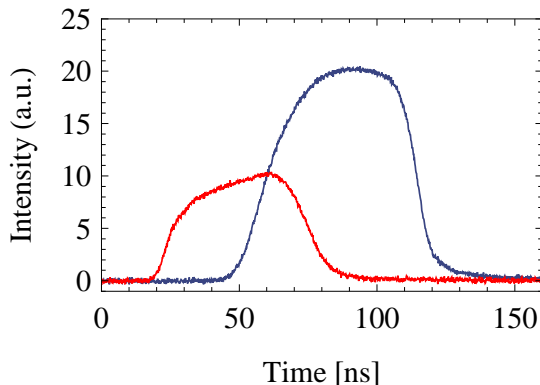


Figure 3.9: The STIRAP-pulses measured with the fast photodiode. Red line: STIRA1, blue line: STIRAP2. The pulse duration T is ~ 55 ns FWHM.

with a fast photodiode. The pulse length is 55ns FWHM for both pulses.

After having passed the AOMs, the lasers are overlapped at a beamsplitter and coupled into a single-mode fiber that guides them to the trap setup. This guarantees a perfect spatial overlap of the two beams. Figure 3.10 shows the optical setup before the trap. In order to be able to choose arbitrary measurement bases (i.e. polarizations) the STIRAP beam has to be oriented parallel to the quantization axis. We send it into the glass cell in opposite direction of the beam of the optical dipole trap. The beam is first widened in a 10:1 telescope and then focused down to the trap center by an achromatic lens of focal length $f = 100$ mm to a waist of $6 \mu\text{m}$. For selecting the atomic measurement basis the polarization of the STIRAP lasers can be turned by a $\lambda/4$ - and a $\lambda/2$ -waveplate that are mounted on stepermotors.

Compensation of the birefringence of the glass cell

It has turned out that the walls of the glass cell show substantial birefringence. They induce a phase shift between the H - and V -polarized components of light that crosses them and thus considerably turn the polarization state of $\pm 45^\circ$ -polarized light. In order to compensate this we have installed a highly birefringent YVO_4 -Yttrium-Orthovanadat crystal ($n_o = 1.94$, $n_e = 2.15$, thickness: $200 \mu\text{m}$) behind the λ -waveplates. Its ordinary and extraordinary axes are oriented parallel to H and V . Tilting the crystal with respect to the beam axis as depicted in figure 3.10 allows to reverse the phase-shift between horizontally and vertically polarized electric field components that is induced by the glass cell.

Pulse intensities

For an efficient transfer the speed of the pulse variation $\dot{\varphi}$ (i.e. their duration) and the Rabi frequencies Ω_1, Ω_2 have to be chosen such that the adiabaticity criterion (3.10)

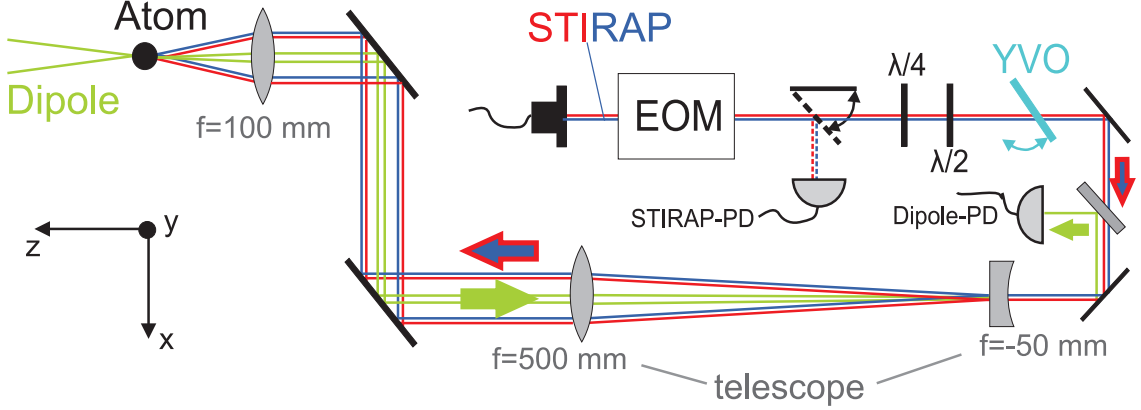


Figure 3.10: Optical setup for focusing the STIRAP beams onto the atom. λ -waveplates choose the atomic measurement basis. The YVO crystal behind them serves as phase compensation plate. A movable mirror can deflect the lasers onto a fast photodiode (PD) for recording the pulse form and intensity. The light from the dipole trap travels in the opposite direction. Behind the telescope a dichroic mirror reflects it onto the photodiode that is used to electronically stabilize its intensity.

is fulfilled. Since the pulse duration is limited by the phase stability of the two lasers, the fulfillment of this criterion now depends on Ω_1, Ω_2 and thus the intensity of the pulses. For the given pulse durations the peak intensities of the pulses must be of the order of a few hundred saturation intensities I_{sat} [27, 18], where $I_{sat1} = 5.98 \frac{\text{mW}}{\text{cm}^2}$ and $I_{sat2} = 17.95 \frac{\text{mW}}{\text{cm}^2}$, respectively (see A.2). The pulse heights at the photodiode (figure 3.9) are chosen such that the resulting Rabi-frequencies Ω_1 and Ω_2 are equal at the pulse maxima.

In order to find the optimal intensity, the atom is first prepared in the superpositions $\frac{1}{\sqrt{2}}(|1, +1\rangle \pm |1, -1\rangle)$. This is done by entangling the atom with a photon and performing a projection measurement on the photon in the H, V -basis. Then a V -polarized STIRAP pulse is applied for which the dark and bright states are $|\Psi_{DV}\rangle = \frac{1}{\sqrt{2}}(|1, +1\rangle - |1, -1\rangle)$ and $|\Psi_{BV}\rangle = \frac{1}{\sqrt{2}}(|1, +1\rangle + |1, -1\rangle)$, respectively. The transfer efficiencies for $|\Psi_{DV}\rangle$ and $|\Psi_{BV}\rangle$ can then be derived from the probabilities to redetect the atom after the subsequent hyperfine state readout. The optimal intensity is found by scanning the pulse intensities and observing these probabilities. Figure 3.11 shows the result of such a scan. The x -axis denotes the intensity of the STIRAP lasers given in their respective saturation intensities I_{sat} . The blue and red lines give the redetection probabilities if the atom was in the bright and dark state, respectively. We are interested in the intensity where the contrast between the redetection probabilities of $|\Psi_{DV}\rangle$ and $|\Psi_{DB}\rangle$ is maximal. As one sees this is the case at about $120 - 140 I_{sat}$. At $400 I_{sat}$ the transfer efficiency of the bright state is

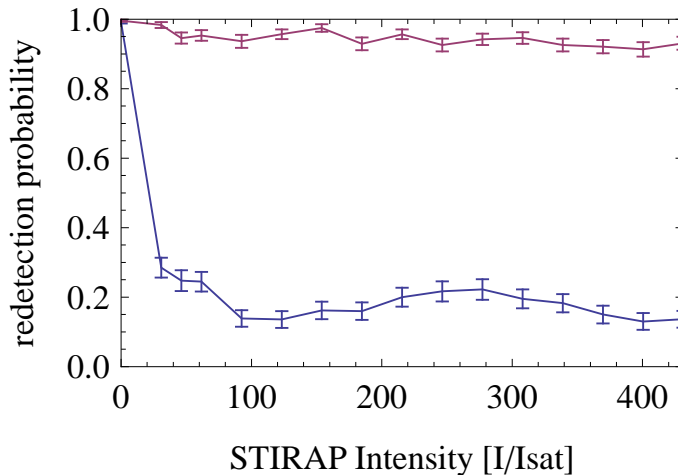


Figure 3.11: Dependence of the STIRAP transfer efficiency on the intensity of the laser pulses. Shown are the probabilities to redetect the atom after the hyperfine state detection if the atom was prepared in the dark state of STIRAP (red line) or the bright state (blue line), respectively.

even higher, but here also the dark state starts to be considerably transferred due to off-resonant coupling to $F' = 2$. For this optimal value the redetection probabilities are:

$$\begin{aligned} \text{dark state} &: 94.9 \pm 0.9 \% & (3.14) \\ \text{bright state} &: 15.7 \pm 1.4 \% \end{aligned}$$

It must be considered that these probabilities also contain the errors caused by the limited accuracy of the hyperfine state detection given in (3.5). In order to obtain the accuracy of the STIRAP process alone - i.e. the probability that the bright state is transferred to $F = 2$ and the dark state not - one must correct (3.14) for these errors. One obtains:

$$\begin{aligned} \text{dark state} &: 96.5 \% & (3.15) \\ \text{bright state} &: 86.8 \% \end{aligned}$$

The transfer efficiency of the bright state is not yet satisfactory for our purposes if compared with what has been achieved in the first trap setup [19]. It cannot be improved by increasing the intensity of the STIRAP lasers due to the off-resonant coupling to $F' = 2$. However, it is possible that further fine-tuning of the temporal shape of the pulses and their time-delay might lead to a better transfer efficiency [38].

Summary

This section described how the Zeeman state of the atom can be read out by state dependently removing the atom from the trap. With this method it is possible perform measurements on the atomic qubit in arbitrary measurement bases by selecting the appropriate polarization of the STIRAP beam. In particular, it became clear that this readout scheme is to be interpreted as a projection of the atomic qubit onto the coherent dark state of the chosen STIRAP polarization.

3.5 Stabilization of the atomic qubit

Our atomic qubit is encoded in a coherent superposition of the Zeeman sublevels $m_F = \pm 1$ of the $F = 1$ ground state. If this state is subject to effects that couple to the quantum number m_F , the coherent phase relation between the Zeeman state becomes time-dependent. These mechanisms of *dephasing* decrease the correlations for measurements on the entangled atom-photon pairs. In order to preserve the correlations the atomic qubit must be stabilized for the time that passes between the creation of the entangled state and the end of the Zeeman state-selective STIRAP process. In total this is a time of about 500 ns. For the envisaged atom-atom entanglement experiment with a distance of 300 m the atomic state has to be stable for at least $1.5 \mu\text{s}$.

This section first describes the two main sources of perturbation of the atomic qubit. Then our method of stabilizing the atomic qubit against these external perturbations is presented.

3.5.1 Mechanisms of dephasing

In our experiment there are mainly two mechanisms that couple to the magnetic quantum number of the atomic state:

- There is an external magnetic field \vec{B} created by e.g. the permanent magnet of the ion getter pump, the 50 Hz of the electric power line, other electric devices as well as the strong currents of the adjacent subway tracks. The static field of the ion getter pump is of the order of $10^2 \dots 10^3$ mG whereas the other sources create field fluctuations of $1 \dots 10^2$ mG [19]. Since the sources are far away from the optical dipole trap compared to its size, the fields can be considered spatially constant over the trapping potential.

According to the Zeeman effect such fields couple to the magnetic moment $\mu = \mu_B \cdot g_F \cdot m_F$ of the atom. Where $\mu_B = 2\pi\hbar \cdot 1.4 \text{ MHz/G}$ is the Bohr magneton and g_F is the Landé factor which equals $-1/2$ for the $F = 1$ hyperfine level.

This coupling leads to an energy splitting of the Zeeman levels. For a field along the quantization axis it is given by:

$$\Delta E_{Zeeman} = \mu \cdot B_z = \mu_B \cdot g_F \cdot m_F \cdot B_z \quad (3.16)$$

- The light of the dipole trap is not exactly linearly polarized mainly due to birefringence of the vacuum glass cell. The induced lightshift $U_{dip}(\vec{r})$ from equation (3.1) then also becomes linearly dependent on $g_F \cdot m_F$. This has the same effect as a space-dependent magnetic field along the quantization axis of the order of 1...10 mG for our polarization errors of 1% and below [19].

All in all these two effects can be summarized in a single time- and space- dependent effective magnetic field \vec{B}_{eff} :

$$\vec{B}_{eff}(\vec{r}, t) = \vec{B}(t) + P \cdot \frac{1}{\mu_B} \frac{\pi c^2 \Gamma}{2\omega_0^3} \left(-\frac{1}{\Delta_{2,F}} + \frac{1}{\Delta_{1,F}} \right) I_\sigma(\vec{r}) \cdot \vec{e}_z \quad (3.17)$$

where I_σ denotes the intensity of the circularly polarized fraction of the dipole trap light and $P = \pm 1$ for σ^+ - and σ^- - polarization, respectively. This effective magnetic field acts on the atomic qubit during the time after the emission of the spontaneously emitted photon until the termination of the STIRAP process and causes it to perform Larmor precessions in the three-dimensional Hilbertspace spanned by $\{|1, -1\rangle, |1, 0\rangle, |1, +1\rangle\}$. The aim of the work described in this section is to reduce the perturbation induced by this effective magnetic field to a minimum. We will try to achieve this by artificially creating a second magnetic field $\vec{B}_{comp} = -\vec{B}_{eff}$ that shall cancel out the original perturbative field.

Classification of the perturbations

Before we start with the compensation procedure we first try to further classify the above mentioned perturbations. For this we have to note that the effective magnetic field has contributions on three different timescales:

1. Constant contributions as for example the field created by the permanent magnet of the ion getter pump. These lead to a *coherent rotation* of the atomic qubit that stays the same during each realization of one experiment of atom-photon entanglement.
2. Contributions that vary for each individual realization of the experiment but stay approximately constant over the duration of one single experiment (“shot-to-shot noise”). These contributions are on the one hand given by fluctuations of the magnetic field that have such a low frequency that they are constant over the duration of one single experiment. On the other hand the contribution of the vector-lightshift induced by the dipole laser varies randomly from

experiment to experiment since it depends on the position of the atom in the trap. These contributions lead to a random rotation of the atomic state for different realizations of the experiment. This kind of perturbation is called *dephasing*.

3. Perturbations that vary within the duration of a single experiment. These are given by fluctuations of the external magnetic field at high frequencies. It has been shown that the amplitude of these fluctuations is negligible for our case [19].

The dynamics of the atomic state in the presence of these contributions can now be divided into two components: A coherent rotation of the atomic spin in the constant field and dephasing due to fluctuations of the field and the effect of the dipole trap. Given a sufficient bandwidth of the compensation mechanism it is in experiment possible to create a compensation field that cancels out the constant contribution of the magnetic field as well as its shot-to-shot fluctuations. It is however impossible to compensate for the contribution of the optical dipole trap.

3.5.2 Method for compensation of external magnetic fields

The mechanism for compensating the external magnetic field works in the following way:

The first step is to stabilize the magnetic field in the vicinity of the atom to a fixed value over many repetitions of the experiment. For this the field fluctuations are measured with a magnetic field sensor. This sensor produces three voltage signals that are proportional to the components of the magnetic field in the three spatial directions. It has a resolution of below one mG and is installed at a distance of about 3 cm from the atom at the exterior of the glass cell. Moreover, three pairs of magnetic coils are installed around the trap - one along each of the spatial axes. These are used to produce the compensation field \vec{B}_{comp} . The signals from the magnetic field sensor are now fed into a feedback loop [19] in which they are compared to three voltages that can be manually chosen by a potentiometer. The feedback loop controls the currents of the magnetic coils such that the signals of the field sensor constantly equal the voltages chosen by the potentiometers. The residual fluctuations of the stabilized field can be monitored by observing the sensor signal. It shows fluctuations with frequencies above 200 Hz and a standard deviation of the peak-to-peak amplitude of 2 mG.

The signals of the magnetic field sensor do not give information about the absolute value of the magnetic field, but only of its variations. In order to find the configuration of the compensation field that exactly cancels the external field it is necessary to try different control voltages chosen by the potentiometers and to observe the

Larmor precessions of the atom in the residual magnetic field. The optimal value is then found if the frequency of the Larmor precessions has been minimized.

3.5.3 Evolution of a spin-1 system in a constant magnetic field

In order to enable a better understanding of the measured Larmor precessions we now give a theoretical description of the behaviour of the atomic spin in the presence of a constant effective magnetic field \vec{B}_{eff} . The Hamiltonian for an atom in the hyperfine state F interacting with \vec{B}_{eff} is given by:

$$\hat{H} = \vec{B}_{eff} \cdot \frac{\mu_B g_F}{\hbar} \hat{\vec{F}} \quad (3.18)$$

$\hat{\vec{F}}$ being the vector operator of the angular momentum for the $F = 1$ space with components $\hat{F}_x, \hat{F}_y, \hat{F}_z$. This operator measures the projection of the atomic angular momentum onto the x, y and z -axis, respectively, and has eigenvalues $\pm 1, 0$. We now write the magnetic field as

$$\vec{B}_{eff} = B_{eff} \left(\sqrt{1 - b_z^2} \cos \phi \cdot \vec{e}_x + \sqrt{1 - b_z^2} \sin \phi \cdot \vec{e}_y + b_z \cdot \vec{e}_z \right) \quad (3.19)$$

with $\phi \in [0, 2\pi]$. A calculation of the eigenstates of \hat{H} represented in the eigenbasis $\{|1, +1\rangle, |1, 0\rangle, |1, -1\rangle\}$ of F_z yields [19]:

$$\begin{aligned} |\Phi_{+1}\rangle &= \begin{pmatrix} \frac{1}{2}(1 + b_z)e^{-i\phi} \\ \frac{1}{\sqrt{2}}\sqrt{1 - b_z^2} \\ \frac{1}{2}(1 - b_z)e^{i\phi} \end{pmatrix} \\ |\Phi_0\rangle &= \begin{pmatrix} -\frac{1}{\sqrt{2}}\sqrt{1 - b_z^2}e^{-i\phi} \\ b_z \\ \frac{1}{\sqrt{2}}\sqrt{1 - b_z^2}e^{i\phi} \end{pmatrix} \\ |\Phi_{-1}\rangle &= \begin{pmatrix} \frac{1}{2}(1 - b_z)e^{-i\phi} \\ -\frac{1}{\sqrt{2}}\sqrt{1 - b_z^2} \\ \frac{1}{2}(1 + b_z)e^{i\phi} \end{pmatrix} \end{aligned} \quad (3.20)$$

With the respective eigenvalues $-\hbar\omega_L, 0, +\hbar\omega_L$. Where $\omega_L := \frac{1}{\hbar} \mu_B g_F B_{eff}$ is the Larmor frequency. With this the time evolution of an arbitrary state $|\Psi\rangle$ in the Schrödinger picture can be written as:

$$|\Psi(t)\rangle = c_{-1}e^{i\omega_L t} |\Phi_{-1}\rangle + c_0 |\Phi_0\rangle + c_{+1}e^{-i\omega_L t} |\Phi_{+1}\rangle \quad (3.21)$$

So the time evolution of $|\Psi\rangle$ is periodic with the Larmor frequency ω_L . This allows to determine the absolute magnitude of the magnetic field \vec{B}_{eff} experimentally by

measuring the time T it takes the atom to perform one Larmor rotation. For a given T , B_{eff} can be calculated from the following formula:

$$|\vec{B}_{eff}| = \frac{2\pi \hbar}{\mu_B g_F} \cdot \frac{1}{T} \quad (3.22)$$

For measurements of the Larmor precession we normally prepare the atom in the dark and bright states $|\Psi_{D_V}\rangle$ and $|\Psi_{B_V}\rangle$ of V -polarized STIRAP. The dynamics of the atomic state are then analysed by reading out the atomic state after a waiting time t with a V -polarized STIRAP pulse. It might be instructive to know in advance what the behaviour of the dynamics of these states look like under different magnetic fields. Let us consider two special cases:

(i) $\vec{B}_{eff} \parallel \vec{z}$, so $b_z = 1$

(ii) $\vec{B}_{eff} \perp \vec{z}$, so $b_z = 0$

We now search the representation of $|\Psi_{D_V}(t)\rangle$ and $|\Psi_{B_V}(t)\rangle$ in the basis (3.20). For this we use their definitions in terms of $|1, \pm 1\rangle$ from table 2.1.

For case (i) the eigenstates (3.20) equal $\{|1, +1\rangle, |1, 0\rangle, |1, -1\rangle\}$ and we obtain:

$$|\Psi_{B_V}(t)\rangle = \frac{1}{\sqrt{2}} e^{-i\omega_L t} (|1, +1\rangle + e^{i2\omega_L t} |1, -1\rangle) \quad (3.23)$$

$$|\Psi_{D_V}(t)\rangle = \frac{1}{\sqrt{2}} e^{-i\omega_L t} (|1, +1\rangle - e^{i2\omega_L t} |1, -1\rangle) \quad (3.24)$$

From these equations one can see, that except for a global phase $e^{-i\omega_L t}$ both states already return into their initial state after *half* a Larmor period since the relative phase between $|1, +1\rangle$ and $|1, -1\rangle$ rotates with $2\omega_L$. Moreover, they do not leave the qubit space $\{|1, +1\rangle, |1, -1\rangle\}$. For example $|\Psi_{B_V}\rangle$ first rotates into $|\Psi_{D_{+45^\circ}}\rangle$ after $\frac{T}{8}$ and then into $|\Psi_{D_V}\rangle$ and $|\Psi_{D_{-45^\circ}}\rangle$ after $\frac{T}{4}$ and $\frac{3}{8}T$, respectively. In the picture of the Bloch-sphere this is a rotation of the atomic spin in the equatorial plane perpendicular to the eigenstates of $\hat{\sigma}_z$.

For case (ii) the situation is more complicated:

$$|\Psi_{B_V}(t)\rangle = \frac{1}{\sqrt{2}} \left(\cos \phi e^{-i\omega_L t} |\Phi_{+1}\rangle - \sin \phi i \sqrt{2} |\Phi_0\rangle + \cos \phi e^{i\omega_L t} |\Phi_{-1}\rangle \right) \quad (3.25)$$

$$|\Psi_{D_V}(t)\rangle = \frac{1}{\sqrt{2}} \left(\sin \phi i e^{-i\omega_L t} |\Phi_{+1}\rangle - \cos \phi \sqrt{2} |\Phi_0\rangle + \sin \phi i e^{i\omega_L t} |\Phi_{-1}\rangle \right) \quad (3.26)$$

Here population of $|1, 0\rangle$ becomes possible and the qubit becomes a ‘‘qutrit’’.

What can be measured in an experiment, is the projection of states (3.23) - (3.26) onto the dark state of the chosen STIRAP polarization. For V -polarization one finds for case (i):

$$|\langle \Psi_{D_V} | \Psi_{B_V}(t) \rangle|^2 = \sin^2 \omega_L t \quad (3.27)$$

$$|\langle \Psi_{D_V} | \Psi_{D_V}(t) \rangle|^2 = \cos^2 \omega_L t \quad (3.28)$$

And for case (ii):

$$|\langle \Psi_{D_V} | \Psi_{B_V}(t) \rangle|^2 = \sin^2 \phi \cos^2 \phi (\cos^2 \omega_L t - 2 \cos \omega_L t + 1) \quad (3.29)$$

$$|\langle \Psi_{D_V} | \Psi_{D_V}(t) \rangle|^2 = \sin^4 \phi \cos^2 \omega_L t + 2 \sin^2 \phi \cos^2 \phi \cos \omega_L t + \cos^4 \phi \quad (3.30)$$

Figure 3.12 shows plots of these functions. For a field of 200 mG parallel to the quantization axis \vec{z} (top left) one finds the pure sinusoidal oscillations given by equations (3.27) and (3.28). After $\sim 3.5 \mu\text{s} = \frac{T}{2}$ the states have performed an entire rotation and have returned to their initial state. In contrast, for a field of same strength along \vec{y} , i.e. $\phi = \frac{\pi}{2}$, (top right) the situation becomes not symmetric. The state $|\Phi_{B_V}(t)\rangle$ from eq. (3.25) is constant in time because it equals the eigenstate $|\Phi_0\rangle$. At the same time $|\Psi_{D_V}(t)\rangle$ oscillates with $2 \cdot \omega_L$ and also populates $|1, 0\rangle$ (see eqns (3.25) and (3.20)). The bottom left plot shows a more general situation with field components along all three spatial axes. The curves are very unsymmetric and it now takes a whole Larmor period until $|\Psi_{B_V}(t)\rangle$ and $|\Psi_{D_V}(t)\rangle$ have returned into their original state.

Finally, the situation in the bottom right demonstrates that sometimes it is not sufficient to analyse Larmor precessions by projecting onto only one dark state: If the field is along the x -axis ($\phi = 0$) the projections of $|\Psi_{D_V}(t)\rangle$ and $|\Psi_{D_H}(t)\rangle$ onto the STIRAP dark state are constant in time and one might suspect that the magnetic field is zero. However, as we can see from eqs 3.25 and 3.26, only $|\Psi_{D_V}(t)\rangle$ is constant in time. It is the eigenstate $|\Phi_0\rangle$ of this field configuration. Whereas $|\Psi_{B_V}(t)\rangle$ still oscillates in the $\{|\Phi_{-1}\rangle, |\Phi_{+1}\rangle\}$ subspace. This subspace is orthogonal to the state on which we project. The state projection then always is zero and the dynamics are not visible. This example shows us that for verifying that the magnetic field is zero along all spatial directions, it is necessary to perform a full state tomography of the atomic qubit [19].

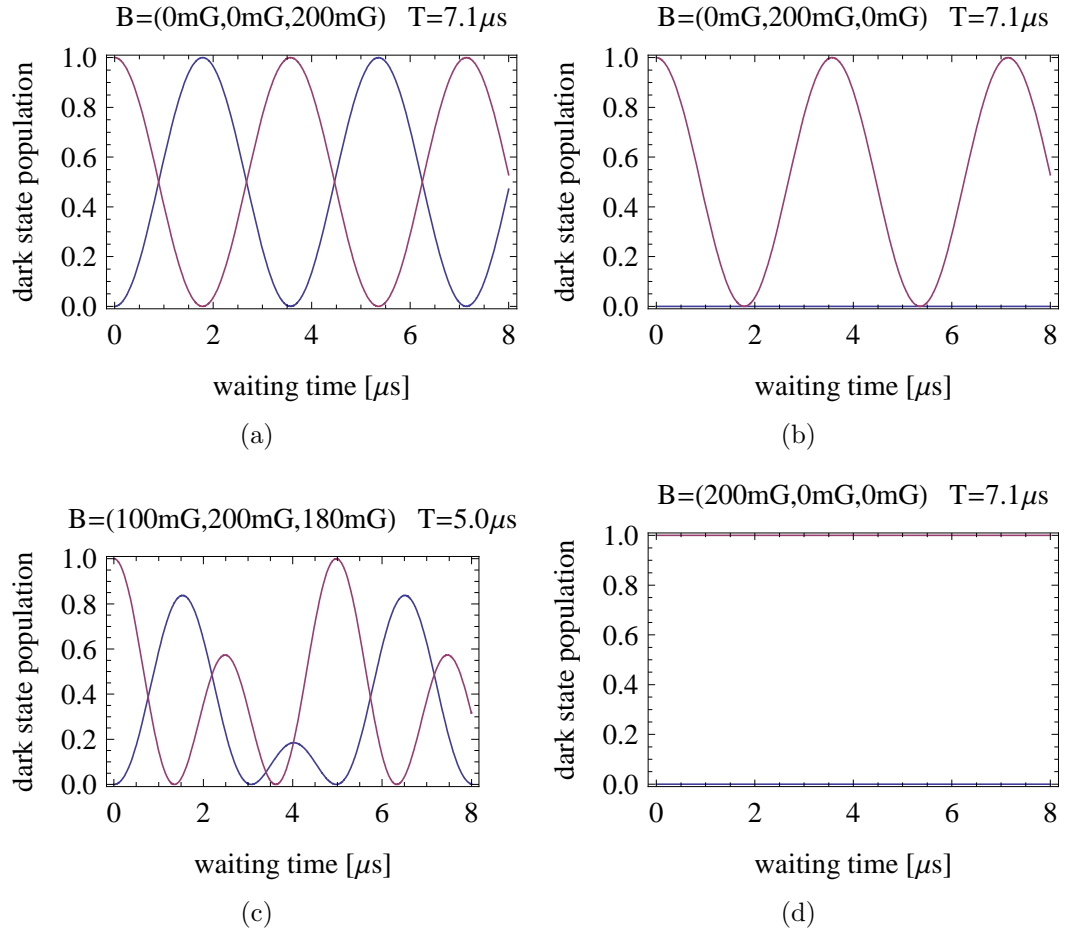


Figure 3.12: Temporal evolution of $|\Psi_{D_V}(t)\rangle$ (red line) and $|\Psi_{B_V}(t)\rangle$ (blue line) given by their projection onto $|\Psi_{D_V}\rangle$ for different field configurations. The specific durations $T = \frac{2\pi}{\omega_L}$ of one Larmor period are indicated above each plot.

3.5.4 Measurements of Larmor precessions

The theoretical model presented in the previous section can help to interpret measurements of Larmor precessions and allows to decide along which axis the magnetic field has to be compensated. But still several iterations are necessary to obtain a satisfactory compensation. In our case, the aim is that the duration of one Larmor precession should be considerably longer than the time that passes between the emission of the decay photon and the end of the STIRAP transfer. Because of delays in the electronics that create the STIRAP laser pulses the STIRAP transfer is performed about 400 – 500 ns after the detection of a photon.

For measuring the Larmor precessions the atom is prepared in the dark and bright state $|\Psi_{D_V}\rangle$ and $|\Psi_{B_V}\rangle$ of V -polarized STIRAP. This is done by entangling the atom with a photon and performing a projection measurement on the photon in the $\hat{\sigma}_x$ -basis. After the detection of the photon a waiting time t is introduced before the creation of the STIRAP pulse. By varying t one observes an oscillation of the probability to redetect the atom after the atomic state detection which is a clear sign that the population of the dark state for the chosen STIRAP polarization oscillates.

The results of such measurements with V - polarized STIRAP are shown in figure 3.13. Figure a) shows the situation before compensation of the magnetic fields. The atomic qubit considerably rotates out of its initial state within less than 500 ns. This can be seen from the fact that already for $t = 0$ the redetection probability for atoms in $|\Psi_{D_V}\rangle$ (red line) has decreased to 0.5. The duration T of one Larmor period is $\sim 2 \cdot 4\mu\text{s}$ from which we conclude that the magnetic field is of about 180 mG.

Figure 3.13(b) shows the situation after the compensation. Now T is about $2 \cdot 60\mu\text{s}$ which gives $B_{eff} \approx 12\text{mG}$. Due to the symmetry between oscillations of $|\Psi_{D_V}\rangle$ and $|\Psi_{B_V}\rangle$ one can conclude that the residual field is along the quantization axis. After about $200\mu\text{s}$ the amplitude of the oscillations decreases to zero and the redetection probabilities approach 0.5. This can be explained by dephasing due to residual fluctuations of the magnetic field and the Zeeman-state dependent lightshift of the dipole trap. On long timescales of several $100\mu\text{s}$ this leads to random rotations of the atomic angular momentum and thus to an entirely mixed state [19].

Finally, figure 3.13(c) shows the behaviour of the atom on short timescales for compensated fields. One sees that for $t = 0$ no rotation out of the original state takes place.

Summary

In this section it was demonstrated that the atomic qubit can be stabilized over a sufficiently long time for performing the atom-photon entanglement experiment. With regard to the envisaged atom-atom entanglement the compensation of the magnetic fields needs further optimization. For this experiment the atomic qubit must be stable for about $3\mu\text{s}$ which also is possible with the presented method.

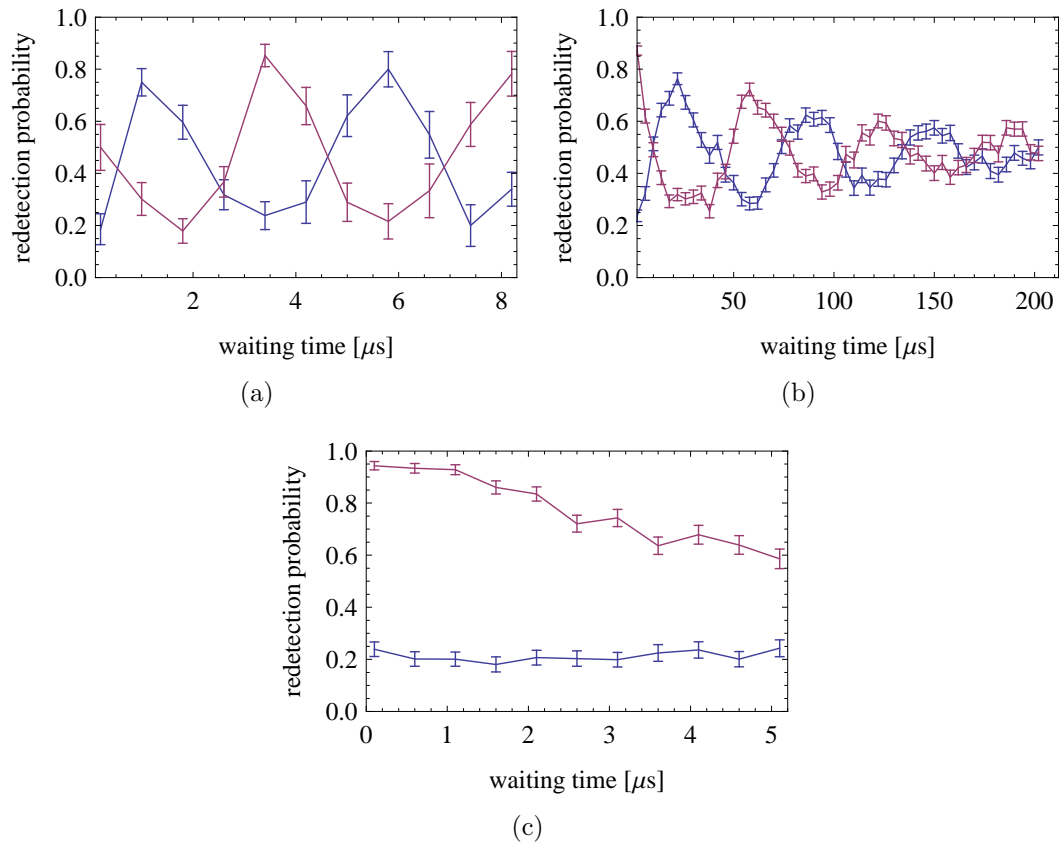


Figure 3.13: Larmor precessions of the atomic states $|\Psi_{D_V}(t)\rangle$ (red line) and $|\Psi_{B_V}(t)\rangle$ (blue line) measured by their projection onto the dark state of V -polarized STIRAP as a function of the waiting time t . a) Before compensation of the magnetic fields. The atomic qubit performs a full precession back into its initial state within $4 \mu\text{s}$. b) and c) After compensation: $T = 2 \cdot 60 \mu\text{s}$. The atomic state is stable for the time that is needed to perform the state readout.

3.6 Optimization of the optical pumping duration

In order to allow for a higher efficiency of the excitation process the atom is first optically pumped into the desired initial state $5^2S_{1/2}, F = 0, m_F = 0$ before every excitation (see figure 3.5(a)). Hence, the duration of the optical pumping process is one of the limiting factors for the creation rate of entangled atom-photon pairs. It is therefore necessary to find the minimal pumping duration with which one still obtains a maximal occupation of the desired $|1, 0\rangle$ ground-state.

As a measure for the efficiency of the pumping process one can take the *excitation efficiency* i.e. the probability to detect a photon after an excitation of the atom. Figure 3.14 shows the results of a measurement, where the dependency of the excitation efficiency on the pumping duration was examined. The pumping duration was varied from 0.5 to 2.9 μs . One observes that the maximal excitation efficiency can be achieved for a pumping duration of about 2 μs . This is less than the 4 μs that were supposed for the calculation of the repetition rate of atom-atom entanglement in [31] and may help increasing the rate of created atom-atom pairs. Besides, the

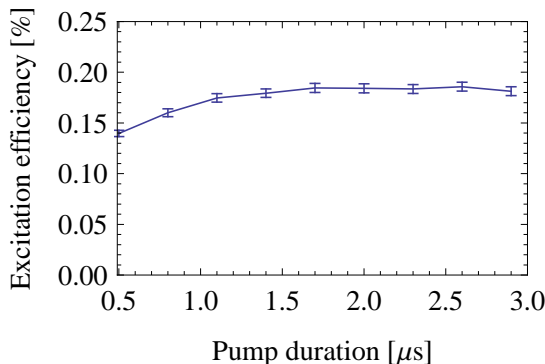


Figure 3.14: Dependence of the excitation efficiency on the duration of the optical pumping period. About 2 μs of optical pumping are necessary in order to achieve the maximal excitation efficiency.

determined optimal pumping duration is by far shorter than the cycle duration of an atomic Larmor precession after compensation of the ambient magnetic field (see previous section). This means that spin rotation out of $|1, 0\rangle$ into $|1, \pm 1\rangle$ does not occur on the timescale of the optical pumping. This would reduce the efficiency of the optical pumping and thus also the excitation efficiency. Moreover, it would make the atom again resonant to the pump lasers and consequently lead to more scattering events and thus more heating than necessary.

3.7 Creation of entanglement

In our experiment the entangled atom-photon pair is created during the spontaneous decay of the atom from the $5^2P_{3/2}, F' = 0, m'_F = 0$ excited state as described in section 2.2.1. For preparing the atom in this state, a laser pulse is applied that is resonant to the transition $S_{1/2}, F = 1, m_F = 0 \rightarrow P_{3/2}, F' = 0, m'_F = 0$ (see the figure below).

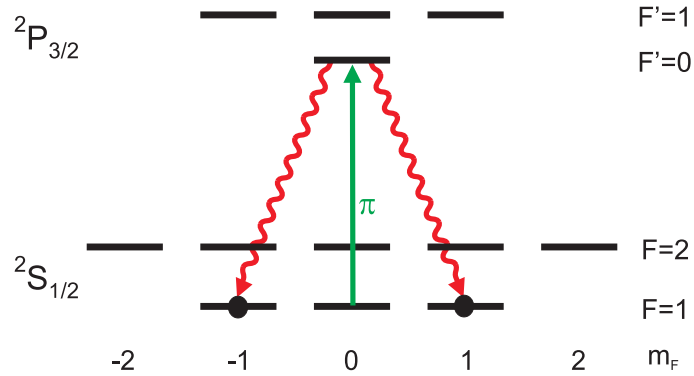


Figure 3.15: Creation of the entangled atom-photon pair. A laser pulse excites the atom to $P_{3/2}, F' = 0, m'_F = 0$ from where the spontaneous decay takes place.

In the following it will be explained how the pulse duration and intensity of the excitation pulse have to be chosen. The following aspects must be considered in this context:

- The preparation of the excited state must be efficient in order to optimize creation-rate of entangled atom-photon pairs.
- Due to imperfect preparation of the initial $|1, 0\rangle$ ground-state, off-resonant excitation from $|1, \pm 1\rangle$ to $|F' = 1, m'_F = \pm 1\rangle$ is possible¹. The resulting decay does not lead to the desired entangled state from eq. (2.15) and thus lowers the fidelity of the prepared state.
- For the two-photon interference experiment the photons must be spectrally indistinguishable. The excitation and decay process must thus happen under identical conditions in both trap setups.

¹Off-resonant excitation via $|1, 0\rangle \rightarrow |F' = 1, m'_F = 0\rangle$ is forbidden by selection-rules

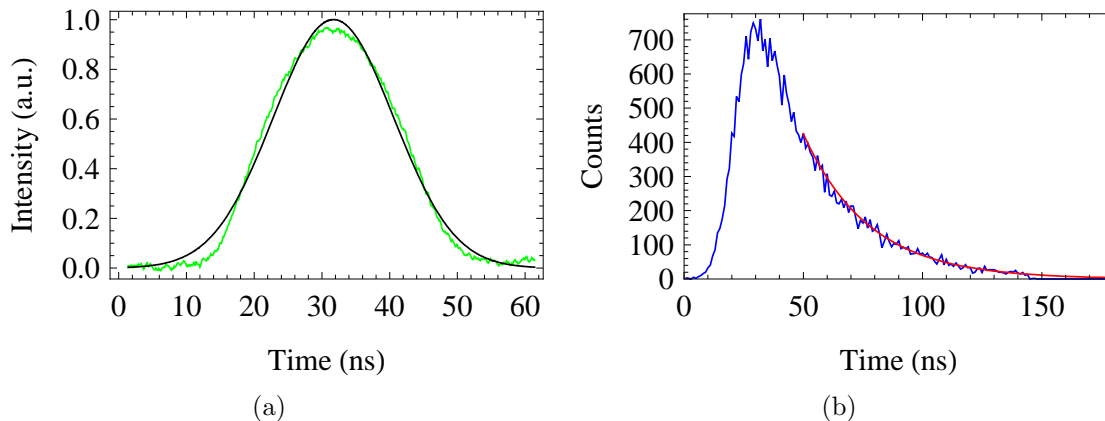


Figure 3.16: a) Temporal shape of the intensity of the excitation pulse (green line). A gaussian fit of the pulse (black line) gives a duration of 21ns FWHM. b) Time distribution of the photon arrival times at the detectors.

3.7.1 Temporal shape of the excitation pulse and the emitted photons

The choice of the temporal shape of the excitation pulse is determined by two factors. On the one hand, one must guarantee that the atom can only scatter one photon over the whole pulse duration. For this, the pulse must be shorter than the lifetime of the $^2P_{3/2}$ excited state of 26.2 ns [22]. On the other hand, for short pulse durations Fourier broadening of the spectral width of the pulse occurs. This increases the probability for off-resonant excitation to neighbouring atomic levels. The relation between the linewidth $\Delta\nu$ of a Fourier-transform limited Gaussian pulse and its pulse duration $\Delta\tau$ is given by

$$\Delta\nu = \frac{2 \ln 2}{\pi \Delta\tau} \quad (3.31)$$

where $\Delta\nu$ and $\Delta\tau$ are the spectral and temporal full-widths at half maximum (FWHM). Our pulse has a duration of 21 ns FWHM and is of approximately gaussian shape as can be seen from figure 3.16(a). The spectrum caused by Fourier broadening is then also given by a Gaussian function. Using equation (3.31) its spectral width is calculated to be 21 MHz FWHM. The distance of the $F' = 0$ excited state to the neighbouring $F' = 1$ state is 72 MHz. This is seven times half of the linewidth caused by Fourier broadening. So for the chosen pulse length this effect does not lead to off-resonant excitation.

Figure 3.16(b) shows a histogram of the arrival times of the emitted photons at the single photon detectors. This measurement graph is directly proportional to the temporal evolution of the occupation of the excited state [40]. The time evolution

in the beginning of the histogram is determined by the interaction with the exciting laser pulse. After 50 ns - when the pulse is off - the evolution is determined by the exponential decay of the excited state. The red line in figure 3.16(b) is an exponential fit that gives a lifetime of the excited state of 27.6 ns which is in good agreement with the theoretical lifetime of 26.2 ns.

3.7.2 Optimal pulse intensity

The aim during the excitation process is to maximize the excitation efficiency. This is achieved if the excitation-pulse leads to a maximal occupation probability of the excited state. In the picture of a two-level atom this corresponds to half of a Rabi oscillation from the ground to the excited state - such a pulse is called a π -pulse. In the following the dynamics of such a Rabi oscillation will be qualitatively illustrated with the help of a simplified model in order to explain the role of the pulse intensity in the excitation process.

Simplified model of a rectangular pulse shape

Let us illustrate the effect of Rabi oscillations in two-level atoms at the simplified model of a rectangular pulse shape. As an additional simplification we neglect the influence of spontaneous decay. Consider that the atom is initially in the ground state. If the pulse is switched on at time $t = 0$ the temporal evolution of the occupation probability $p_{exc}(t)$ of the excited state is given by [39]

$$p_{exc}(t) = \sin^2\left(\frac{\Omega_{Rabi}}{2} t\right) \quad (3.32)$$

where Ω_{Rabi} is the Rabi frequency. Since in our case the pulse duration is limited by the lifetime of the excited state the Rabi frequency is the only parameter that can be varied in order to maximize p_{exc} . It is determined by the intensity I of the incident light field. For $I = const$ the relation between the intensity and the Rabi frequency is given by [22]

$$\frac{I}{I_{Sat}} = 2 \left(\frac{\Omega_{Rabi}}{\Gamma}\right)^2 \quad (3.33)$$

where $\Gamma = 2\pi \cdot 6.07$ MHz is the decay rate of the ${}^2P_{3/2}$ excited state.

Although the model of a rectangular pulse cannot exactly be applied to our case of a Gaussian pulse, it still allows for a good qualitative understanding of the relation between the pulse intensity and p_{exc} . As one can see from the above equations, for increasing intensity the population of the excited state increases until it reaches its maximum for $\Omega_{Rabi} \cdot t = \pi$ - hence the name π -pulse. Here the occupation probability of the excited state is 1. For higher intensities more than half of a Rabi-period is

performed and p_{exc} decreases again. Using equation (3.33) one can derive that for a pulse duration t a π -pulse is obtained for

$$I = 2\pi^2 \left(\frac{1}{t \cdot \Gamma} \right)^2 \cdot I_{sat} = 2\pi^2 \left(\frac{\tau}{t} \right)^2 \cdot I_{sat} \quad (3.34)$$

Where Γ has been replaced by the lifetime of the excited state $\tau = \frac{1}{\Gamma}$. In our case the pulse is 21 ns long. For this duration equation (3.34) yields that an intensity

$$I \approx 30 \cdot I_{sat} \quad (3.35)$$

would be necessary to perform a π -pulse. For our gaussian pulse the exact form of the temporal evolution of p_{exc} will differ from the sinusoidal behaviour of equation (3.32) and also the necessary peak pulse intensity will differ from the value determined above. Moreover, in the presence of spontaneous decay the maximal occupation of the excited state is never 1 as in the ideal situation without spontaneous decay. However, the model gives already an idea of the order of magnitude of the necessary intensity.

Experimental determination of the optimal pulse intensity

Besides the fact that our pulse is not rectangular there is the problem that the exact intensity of the pulse at the position of the atom is unknown due to uncertainties in the beam adjustment. Thus the optimum pulse intensity has to be found experimentally. Therefore the laser power is scanned and the resulting excitation efficiency is measured. Figure 3.17 shows the result of such a measurement. The indicated intensities are the peak intensities of the pulse given in terms of the saturation intensity I_{sat} of the $S_{1/2} |F = 1, m_F = 0\rangle \rightarrow P_{3/2} |F' = 0\rangle$ -transition, where $I_{sat} = 5.008 \frac{\text{mW}}{\text{cm}^2}$ (see A.2). As one can see from the figure about forty saturation intensities are needed in order to achieve the maximal excitation efficiency of 2.2 – 2.4 ‰. This is of the same order of magnitude as what was calculated with the model of a rectangular pulse.

Moreover, one observes in figure 3.17 that above the optimal intensity the excitation efficiency decreases again. This is because for higher laser powers one performs more than a π pulse and the atom partially rotates back into the ground state before spontaneous decay takes place.

The presented measurement was performed with stabilized compensated magnetic fields that allow for a higher efficiency of the preparation of the initial ground state $F = 1, m_F = 0$ by the optical pumping process (see last section). Before the fields had been compensated, the excitation efficiency was considerably lower and showed strong variations in time. Moreover, this measurement was already performed with the dipole trap switched off during the excitation and spontaneous decay. This scheme is going to be presented in the following.

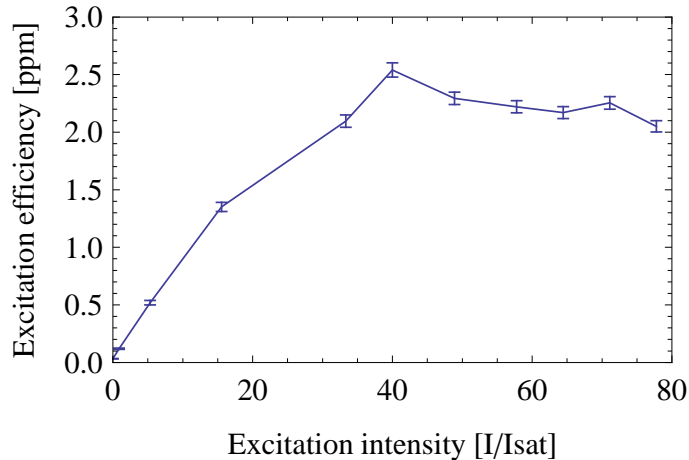


Figure 3.17: Dependence of the excitation efficiency on the laser intensity. About forty saturation intensities are necessary in order to obtain the maximal excitation efficiency.

3.7.3 Creating spectrally indistinguishable photons

We now follow the proposal from 2.3.2 to switch off the dipole trap during the excitation and spontaneous emission of the photon. This shall help to eliminate the spectral broadening of the emitted photons due to the thermally distributed lightshift in the potential of the dipole trap. The only mechanism that leads to incoherent broadening of the photons is then Doppler broadening, which is due to the thermal velocity distribution of the atom.

For creating the spectrally indistinguishable photons the trap is switched off 30 ns before the excitation pulse reaches the atom. The trap then stays turned off for ~ 200 ns until the emission of the photon is completed.

In the previously used scheme in which the trap is on during the excitation, the frequency of the laser is detuned with respect to the $S_{1/2} |F = 1\rangle \rightarrow P_{3/2} |F' = 0\rangle$ -transition in order to correct for the average lightshift of 28 MHz that is induced by the dipole laser. However, if the trap is switched off during the excitation, this is no more the case and the frequency has to be adjusted accordingly. In order to get a better picture of the dependence of the excitation process on the laser frequency, scans of the laser frequency were performed and the resulting excitation efficiency was measured. The results can be seen in figure 3.18. The x -axis values are the detuning of the laser frequency with respect to the transition frequency of $|F = 1\rangle \rightarrow |F' = 0\rangle$ for an atom in free space - i.e. without lightshift.

With the dipole trap off (blue curve) there is a maximum of the excitation efficiency for zero detuning which corresponds to resonant excitation to $|F' = 0\rangle$. A second

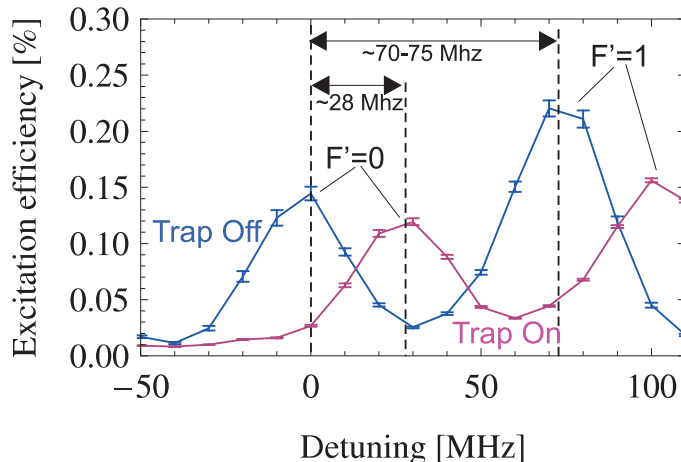


Figure 3.18: Dependence of the excitation efficiency on the laser frequency with the dipole trap off and on during the excitation. The two resonances can be attributed to excitation to $|F' = 0\rangle$ and $|F' = 1\rangle$, respectively. For the case “trap on” the resonances are displaced by the lightshift of 28 MHz with respect to the case “trap off”.

maximum appears for a detuning of $\sim 70\text{--}75$ MHz. At this point the laser is resonant to $|F' = 1\rangle$. The measured distance between the lines is in good agreement with the theoretical energy distance of 72 MHz.

A similar curve is obtained for excitation with the dipole trap on (red curve). Here, however, the maxima are shifted to higher frequencies due to the lightshift of 28 MHz.

During these frequency scans the atomic hyperfine state detection (section 3.4.1) was performed after every photon detection in order to determine the fraction of atoms which decay into the $F = 2$ ground state. Due to selection rules such a decay is only possible if the atom has been excited to the $F' = 1$ level. So the probability to redetect the atom after the hyperfine state readout can serve as a measure for excitation to $F' = 1$. Figure 3.19 shows the probability of the atom to be redetected in the trap after the hyperfine state readout as a function of the excitation laser frequency. On resonance with the transition to $|F' = 0\rangle$ the probabilities are almost 1 for the case of trap on as well as trap off. On resonance with the transition to $F' = 1$ the probability is considerably smaller - at about $80 \pm 2\%$. So apparently after $80 \pm 3\%$ of the decays from $F' = 1$ the atom ends up in $F = 2$. This value can be explained with the branching ratio between the decays from $F' = 1$ into the two hyperfine ground states. The Clebsch-Gordon coefficients for decay from $F' = 1, m'_F = \pm 1$ into $F = 1$ and $F = 2$ are $\sqrt{\frac{5}{24}}$ and $\sqrt{\frac{1}{24}}$, respectively [22]. The

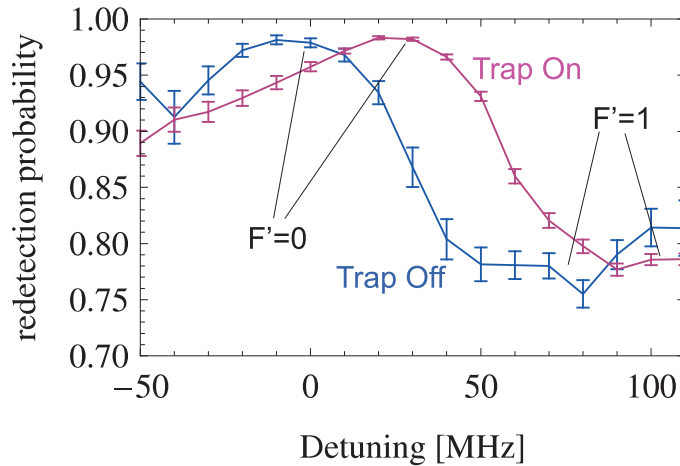


Figure 3.19: Redetection probabilities of the atom after the atomic hyperfine state readout as a function of the excitation laser detuning. On resonance with the $|F' = 1\rangle$ -level the redetection probabilities are lower because decay into $|F = 2\rangle$ occurs.

ratio of the photons that decay into $F = 1$ or $F = 2$ is then given by

$$\begin{aligned}
 F = 1 : & \quad \frac{\frac{5}{24}}{\frac{5}{24} + \frac{1}{24}} \approx 83.3\% \\
 F = 2 : & \quad \frac{\frac{1}{24}}{\frac{5}{24} + \frac{1}{24}} \approx 16.7\%
 \end{aligned} \tag{3.36}$$

since the proportion of photons that decay via a given channel is proportional to the square of the respective Clebsch-Gordan coefficient. One sees that the measured branching ratio is in good agreement with the theoretically expected value.

Width of the resonance lines and hints for off-resonant excitation

As we see from figure 3.18, the width of the resonances for excitation to $|F' = 0\rangle$ and $|F' = 1\rangle$ is of about $\sim 35 - 40$ MHz FWHM. This is about six times the natural linewidth of the D_2 -line of 6.07 MHz. As it was stated in the last section this cannot be explained by spectral Fourier broadening of the excitation laser pulse. By the fact that the resonances are also broad for the case “trap off”, lightshift broadening can be excluded as well. It could be shown in numerical calculations [41] for a pulsed excitation with the pulse shape from fig. 3.16(a) that the linewidth strongly depends on the laser intensity. The measured linewidths could be reproduced with this program for the intensities we use in experiment (see measurement in figure 3.17). It thus can be concluded, that the measured linewidths are caused by saturation broadening.

There is a considerable overlap of the two lines so that off-resonant excitation to $|F' = 1\rangle$ cannot be excluded even on resonance with the transition to $|F' = 0\rangle$.

As described above a reduced probability to redetect the atom after the hyperfine state readout could serve as a measure for off-resonant excitation. It can be seen in figure 3.19 that the probability is not exactly 1 on resonance with $F' = 0$ but only $98.4 \pm 0.5\%$. However, due to the errors of the detection accuracy of the $F = 1$ hyperfine ground state of $98.3 \pm 1.3\%$ (see eq. (3.5)), no definite conclusion can be drawn from the reduced redetection probabilities.

Atom losses by switching the trap off

In principle there is a possibility that the atom moves out of the region of the trapping potential during the time the trap is switched off and that it is not recaptured when the trap is switched on again. This is however very unlikely which becomes evident if one compares the trap-off time of 200 ns with the cycle duration of one oscillation of the atom in the trapping potential: Even for oscillations along the radial direction (where the trap frequency is the highest - see section 3.2) the cycle duration is $\frac{1}{65.3 \text{ kHz}} = 15.3 \mu\text{s}$. This is almost two orders of magnitude larger than the trap-off time. Hence, it can be assumed that the atom is recaptured at almost the same place at which it was released.

This is confirmed by the measurement in figure 3.19. Here it can be seen that within the errors the redetection probabilities at resonance with the $|F' = 0\rangle$ level are the same for the cases trap on and trap off.

Summary

This section explained the dependency of the excitation process on the two characterizing parameters of the excitation pulse given by the pulse duration and the pulse intensity. We also presented a scheme for creating spectrally indistinguishable photons by switching the dipole trap off during the excitation and spontaneous decay of the atom. It was shown, that with an optimized pulse intensity of about $40 \cdot I_{sat}$ excitation efficiencies of $2.2 - 2.4\%$ can be reached with this scheme. This is the same efficiency that has been reached without switching of the trap. Moreover, it was proven that there are no atom losses due to the switching of the dipole trap.

In measurements of the linewidth of the transitions $F = 1, m_F = 0 \rightarrow F' = 0, m'_F = 0$ and $F = 1, m_F = \pm 1 \rightarrow F' = 1, m'_F = \pm 1$ it was observed that there is a considerable overlap between the lines. Numerical calculations showed that this is due to saturation broadening caused by the high intensities of the excitation pulse. This makes off-resonant excitation to $F' = 1, m'_F = \pm$ possible which would lead to a reduction of the fidelity of the entangled atom-photon state. A method was presented with which the amount of off-resonant excitation can be measured via the occupation of the $F = 1$ -state after the spontaneous decay. However, in order to apply this method the detection accuracy of the $F = 1$ hyperfine state has to be optimized first.

3.8 Measurement of atom-photon correlations

All the necessary experimental steps for creating and verifying entanglement between the Zeeman-state of a single ^{87}Rb -atom and the polarization state of a single photon have been introduced in the course of this chapter. With these tools at hand it is now possible to perform measurements on the two-particle system that reveal the correlations that are the characterizing property of entangled states. In order to test whether the atom-photon pair is entangled, the fidelity of the entangled state will be determined from these measurements.

3.8.1 Choice of the measurement bases and expected correlations

In order to prove entanglement of the atom-photon pair it is necessary to perform measurements on the photon and the atom in two complementary measurement bases. For our setup the experimentally easiest way is to analyze the atom and the photon in the equatorial plane of the Bloch sphere. The representation of a pair of orthogonal states in this plane in the $\hat{\sigma}_z$ -basis is given by:

$$|0_\alpha\rangle = \frac{1}{\sqrt{2}} (|0\rangle_z + e^{i2\alpha} |1\rangle_z) \quad (3.37)$$

$$|1_\alpha\rangle = \frac{1}{\sqrt{2}} (|0\rangle_z - e^{i2\alpha} |1\rangle_z) \quad (3.38)$$

In the picture of the Bloch sphere 2α is the phase angle between $|0\rangle_x$ and $|0_\alpha\rangle$ and $|1_\alpha\rangle$, respectively (see figure 2.1). For the photon α can be varied by turning a $\lambda/2$ -plate in front of the PBS (see figure 3.6(a)). The PBS transmits H -polarized photons and reflects V -polarized photons. If the ordinary and extraordinary axes of the $\lambda/2$ -plate are turned by an angle $\frac{\alpha}{2}$ with respect to H and V then a detection of the photon at APD 1 or APD 2 projects it onto state (3.37) or (3.38), respectively. The atomic measurement basis is given by the polarization of the STIRAP lasers. According to equations (3.11) and (3.12) the beams must be linearly polarized at an angle α with respect to the horizontal plane (see figure 2.3(b)) if one wants to project onto the STIRAP dark-state (3.37). The polarization is set with a rotatable $\lambda/2$ -plate (see figure 3.10). We call a measurement in this basis a measurement under the angle α because in real space (i.e. not on the Bloch sphere) α is the angle between the photon- and STRIAP-polarization with respect to the horizontal plane.

Expected correlation curves

We now derive the correlations between the measurement results that are to be expected for the entangled state given in equation (2.15). For this one must rewrite

the entangled state in the basis states (3.37) and (3.38):

$$|\Psi^+\rangle = \frac{1}{2} \left[(|\sigma^+\rangle + e^{i2\alpha} |\sigma^-\rangle) (|1, +1\rangle - e^{i2\alpha} |1, -1\rangle) + (|\sigma^+\rangle - e^{i2\alpha} |\sigma^-\rangle) (|1, +1\rangle + e^{i2\alpha} |1, -1\rangle) \right] \quad (3.39)$$

We are interested in the probability that the atom is in the STIRAP dark state $|0_\beta\rangle_{At}$ if the photon has been projected onto $|0_\alpha\rangle_{Ph}$ or $|1_\alpha\rangle_{Ph}$, respectively. These probabilities are given by

$$\left| \left({}_{At}\langle 0_\beta | {}_{Ph}\langle 0_\alpha | \right) |\Psi^+\rangle \right|^2 = \sin^2 \Delta\phi \quad (3.40)$$

$$\left| \left({}_{At}\langle 0_\beta | {}_{Ph}\langle 1_\alpha | \right) |\Psi^+\rangle \right|^2 = \cos^2 \Delta\phi \quad (3.41)$$

Where $\Delta\phi = \beta - \alpha$ is the angle between the STIRAP and photon polarization. According to these equations the measurement outcomes for atom and photon are strictly anti-correlated for parallel measurement bases. This means that if the photon is found in $|1_\alpha\rangle$ the atom is always found in $|0_\alpha\rangle$ and vice versa. If the photon-basis is rotated and the atom-basis is fixed the dark state population of the atom and thus its probability to be redetected after the atomic state readout oscillate between 0 and 1.

The peak-to-peak amplitude of these oscillations is called the *visibility* v of the correlation curves. Ideally it is 1 for a maximally entangled state such as our Bell-state. In experiment it is however reduced. Reasons for this are imperfections in the state readout of the particles but also errors during the creation of the entangled state which in our case arise for example from off-resonant excitation to the excited hyperfine level $5^2P_{3/2}F' = 1$.

3.8.2 Experimental sequence

Figure 3.20 depicts the laser sequence that is used to experimentally create and verify atom-photon entanglement. This pattern uses the optimized pumping duration of $2 \mu\text{s}$. After ten pump-excitation cycles the atom is cooled for $400 \mu\text{s}$. During the excitation and subsequent spontaneous decay the dipole trap is switched off for a time window of 200 ns. Conditioned upon the detection of a photon at the APDs the atomic state readout is initialized. On average the atom is removed from the trap by the atomic state detection in 50% of the cases. Thus the loading rate of the trap is the dominating factor for the repetition rate of the atom-photon entanglement experiment. Under ideal conditions about 80 to 100 entangled atom-photon pairs per minute can be generated and analyzed. At this rate error bars on the order of 1 to 5 percent at the points of maximal visibility can be achieved for measurement times of about 3 to 15 minutes per basis setting.

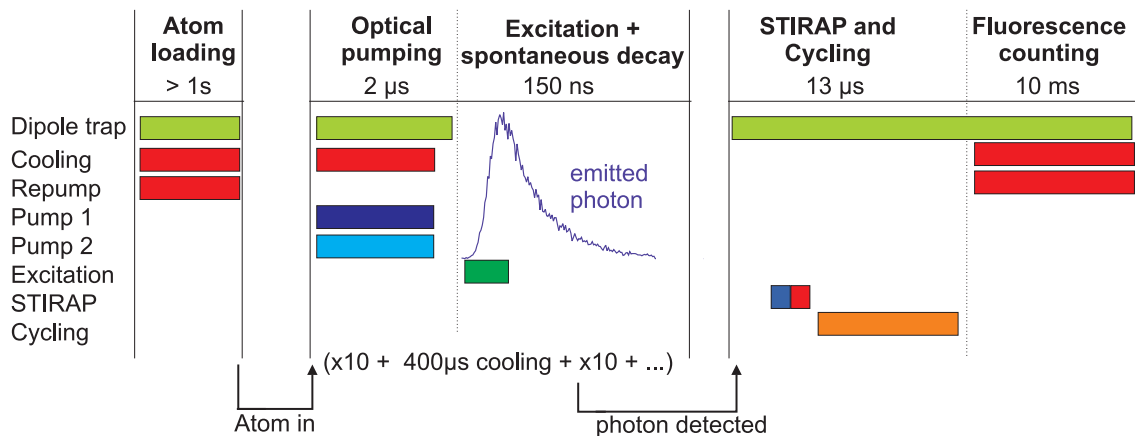


Figure 3.20: The three patterns of laser sequences for performing the atom-photon entanglement experiment with compensated magnetic fields and their respective durations. After an atom has been loaded into the ODT repeated optical pumping and excitation are performed. Conditioned upon the detection of a photon from the spontaneous decay the atomic state readout is initialized.

3.8.3 Results

In the following we present results of measurements of atom-photon correlations. During all measurements the atomic measurement basis was kept fix. The photonic $\lambda/2$ -plate was rotated from $\alpha/2 = 0$ to $\alpha/2 = 90^\circ$ in steps of 11.25° (i.e. in the picture of the Bloch sphere the basis was rotated by 2π in the equatorial plane). The measurement setting is changed after one minute so that long term drifts of experimental parameters are distributed equally among all settings of a measurement run.

Measurements without compensated magnetic fields

First correlation measurements were performed without actively stabilized magnetic fields. Therefore it was necessary that the STIRAP transfer happens very shortly after the excitation process. In order to achieve this the STIRAP process was not conditioned upon the detection of a photon since this retards the STIRAP laser pulse by 400 – 500 ns due to electronic delays of its AOM-drivers etc. Instead, the pattern generator produced a STIRAP pulse during every pump-excitation cycle. The time delay was chosen such that the STIRAP laser pulse reaches the atom within ~ 30 ns after the atom has completely decayed. The subsequent hyperfine state detection can still be carried out conditioned upon the detection of a photon since the hyperfine levels after the STIRAP process are stable against mixing due to magnetic fields. With this method it was possible to calibrate the STIRAP intensity given in section 3.4.4 and to compensate the birefringence of the glass cell by tilting

the YVO-crystal in the STIRAP setup.

Figure 3.21 presents results of these measurements. Shown are the probabilities that the atom is redetected after the atomic state readout when the angle of the photonic state detection is rotated. The blue and red lines correspond to events where the photon was detected at APD 1 or at APD 2, respectively. Figure a) shows correlations for V -polarized STIRAP. One observes the sinusoidal behaviour predicted by equations (3.40) and (3.41). The visibility is 74% and 79% for the blue and red data set, respectively. Due to the birefringence of the glass cell the visibility is considerably worse for a STIRAP-polarization of $+45^\circ$ - see figure b). Here the YVO crystal is in a neutral position where it does not induce a phase shift between H and V . Figures c) and d) show correlations where the crystal was tilted by an angle of 10 and 12 degrees with respect to the neutral position. One observes that the visibility of the correlations is very sensitive to the tilting angle. But the measurement in figure d) proves that it is possible to achieve similar visibility for both complementary atomic measurement bases by correctly tilting the YVO crystal.

Measurements with compensated magnetic fields

By performing the STIRAP transfer very shortly after the atomic decay (as it was described in the preceding paragraph) it was possible to optimize the STIRAP intensities such that the two orthogonal dark and bright states of STIRAP can be distinguished best. The resulting good transfer efficiency of the STIRAP process was necessary for the Larmor measurements presented in section 3.5. With the compensated magnetic fields it is now possible to carry out the STIRAP process only if the excitation was followed by the detection of a photon. This has several advantages compared to an unconditioned STIRAP. With unconditioned STIRAP the atom is transferred to the $|F = 2\rangle$ hyperfine level in on average 50% of the cases where no photon has been detected after the excitation. In these cases the transfer is unnecessary and leads to the problem that during the next optical pumping phase more scattering events are needed in order to pump the atom back into the desired $|1, 0\rangle$ -state. Therefore a longer duration of the optical pumping is necessary in order to achieve the maximal excitation efficiency. Another problem is that the additional scattering events lead to a stronger heating of the atom and thus more cooling phases between the pump-excitation cycles are necessary to allow for long lifetimes of the atom.

The atom-photon correlations that were measured with conditioned STIRAP are shown in figure 3.22. The visibilities are 71% and 65% for V and $+45^\circ$ -polarized STIRAP, respectively. This is less compared to figures 3.21 a) and d) which can be explained by a less optimal STIRAP transfer efficiency during this experimental run and less optimized birefringence of the glass cell. It is not caused by the instability of the atomic qubit due to residual magnetic fields.

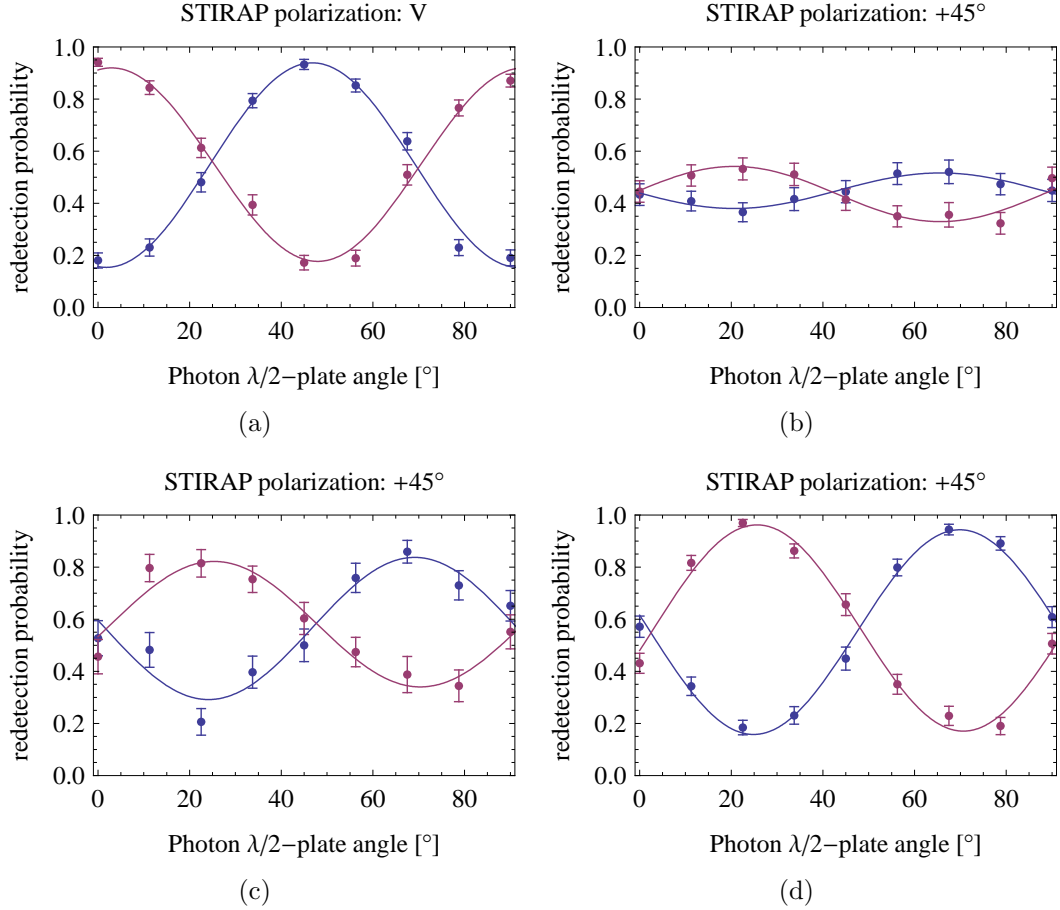


Figure 3.21: Atom-photon correlations without compensated magnetic fields. Shown are the probabilities that the atom is redetected after the atomic state readout when the angle of the photonic state detection is rotated in the equatorial plane of the Bloch sphere. Blue and red lines correspond to events where the photon was detected at APD 1 and APD 2, respectively. One observes the predicted sinusoidal dependence. In figure a) STIRAP was V-polarized. Figures b)-d) show measurements for +45°-polarized STIRAP. The low contrast in figure b) is due to the birefringence of the glass cell. In figures c) and d) the birefringence could be compensated by tilting the YVO crystal with respect to its neutral position by 10° and 12°, respectively.

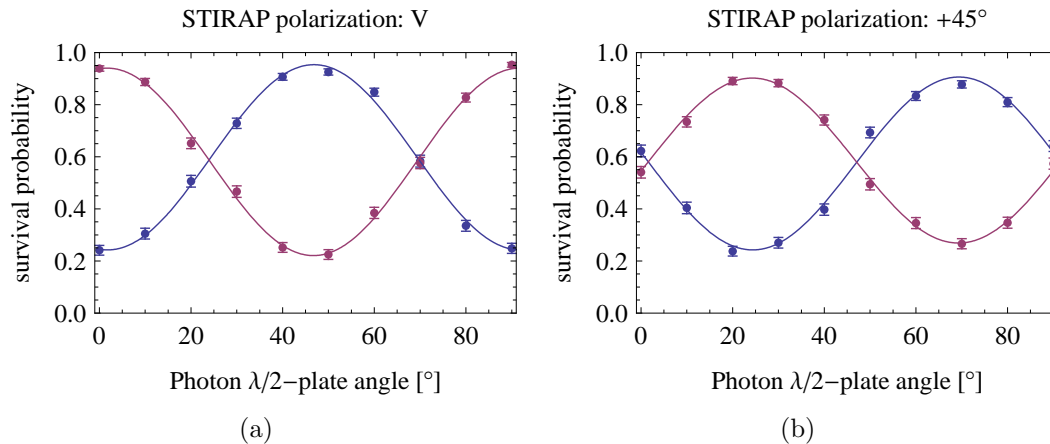


Figure 3.22: Atom-photon correlations with compensated magnetic fields in the two complementary atomic measurement bases V and $+45^\circ$.

Fidelity of the entangled atom-photon state

As a proof that the atom-photon pair is entangled one can estimate the fidelity of the prepared state with respect to the desired $|\Psi^+\rangle$ -state and apply the criterion for entanglement presented in equation (2.11). For this we write the density matrix of the prepared state in the form (2.9):

$$\rho = p \cdot |\Psi^+\rangle\langle\Psi^+| + \frac{(1-p)}{4} \cdot \hat{\mathbb{1}} \quad (3.42)$$

The probability p that the atom is in the desired $|\Psi^+\rangle$ -state can be derived from the visibility of the correlation curves in the following way: Consider two pure atom-photon states $|\phi_1\rangle$ and $|\phi_2\rangle$ with:

$$\begin{aligned} |\phi_1\rangle &= |a\rangle_{At} |b\rangle_{Ph} \\ |\phi_2\rangle &= |a\rangle_{At} |c\rangle_{Ph} \end{aligned}$$

where the photonic states $|b\rangle_{Ph}$ and $|c\rangle_{Ph}$ shall be orthogonal. The overlap of these states with the prepared state ρ is given by $\langle\phi_1|\rho|\phi_1\rangle$ and $\langle\phi_2|\rho|\phi_2\rangle$. It corresponds to the probability of finding the atom in state $|a\rangle_{At}$ if the photon has been projected onto $|b\rangle_{Ph}$ or $|c\rangle_{Ph}$, respectively. These are the two redetection probabilities in the correlation measurements for the specific photonic basis $|b\rangle_{Ph}, |c\rangle_{Ph}$ and STIRAP dark state $|a\rangle_{At}$. If the photonic and atomic measurement bases are parallel, then the difference between these overlaps equals the visibility v :

$$\langle\phi_1|\rho|\phi_1\rangle - \langle\phi_2|\rho|\phi_2\rangle = v \quad (3.43)$$

On the other hand, inserting (3.42) into (3.43) gives:

$$p |\langle\phi_1|\Psi^+\rangle|^2 - p |\langle\phi_2|\Psi^+\rangle|^2 = p \cdot 1 - p \cdot 0 = p \quad (3.44)$$

due to the strict correlations for measurements on a maximally entangled system in parallel bases. So we have:

$$p = v \tag{3.45}$$

With this (2.10) can be written as:

$$F = \frac{1 + 3v}{4} \tag{3.46}$$

For the mean visibility of 66 % from the measurement with compensated magnetic fields we obtain a fidelity of $F=0.745$ which is larger than 0.5. So the prepared atom-photon state is clearly entangled.

Summary

It was shown in this section that with the current trap setup it is possible to generate an entangled pair of a single atom and a single photon. The theoretically expected correlations for the $|\Psi^+\rangle$ -state have been reproduced in two complementary bases. However, the visibilities of the measured correlations still need further optimization. In the first trap setup visibilities of $\sim 90\%$ were achieved [19]. Currently the transfer efficiency of the STIRAP process is clearly the limiting factor for the visibility. Polarization errors are apparently small, otherwise the projection onto the dark state would be less accurate.

4 Temperature measurement of a single trapped atom

The energy of the single atom in the dipole trap is an important parameter in several parts of the atom-photon experiment. For higher temperatures the linewidth of atomic transitions is increasingly broadened due to the lightshift broadening induced by the dipole laser beam. By this, unwanted off-resonant excitation to neighbouring atomic levels becomes more probable. Moreover, also photons that are emitted by the atom are spectrally broadened, which can be a problem for realizing two-photon interference experiments with photons from two trapped atoms [42, 43, 26].

In the context of other single-atom experiments [44, 45] the mean energy of an atom, which has been loaded from a magneto-optical trap into an optical dipole trap and which is cooled there by means of Doppler cooling techniques, has already been examined. It was shown that the energy distribution of the single atom follows the one of an ensemble of classic three dimensional harmonic oscillators at temperature T . Thus it is justified to speak of the “temperature of a single atom” - a term that is usually used for ensembles of many particles.

This chapter presents a method for determining the temperature of a single atom trapped in an optical dipole trap. This is achieved by measuring its energy distribution by instantaneously lowering the trap potential and observing how often the atom can be redetected after the trap has been raised to its initial depth. By comparing the measurement with theoretical predictions the temperature of the atom can be derived.

4.1 Method

Our method for measuring the temperature of the atom is the following: After a single atom has been loaded into the ODT as described in section 3.2, the cooling and repump lasers of the MOT are switched off. The maximal trap depth $U_0 = 1.5$ mK of the ODT is then instantaneously lowered from its standard value U_0 to $x \cdot U_0$, where $0 \leq x \leq 1$ (see figure 4.1). This is achieved by appropriately decreasing the intensity of the dipole laser. Instantaneously means in this context that the time needed for lowering the trap must be shorter than the period of one harmonic oscillation in the trapping potential. This is necessary to avoid adiabatic cooling as it would occur for

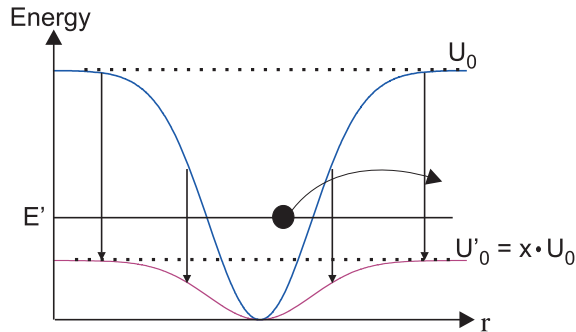


Figure 4.1: Scheme of the temperature measurement of a single atom: The maximal trap depth $U_0 = 1.5$ mK is instantaneously reduced to $U'_0 = x \cdot U_0$ and the atom loses $(1 - x)$ of its original potential energy. If its total energy E' after the lowering of the trap is larger than U'_0 it leaves the trapping potential.

a slow lowering of the potential [44]. During this process the potential energy U of the atom is instantaneously reduced to the fraction x of its original value, whereas its kinetic energy E_{kin} stays constant.

$$\begin{aligned} U' &= x \cdot U \\ E'_{kin} &= E_{kin} \end{aligned}$$

The total energy E' shortly after the lowering is then

$$E' = U' + E'_{kin} = x \cdot U + E_{kin}$$

During the time the trap is lowered, the atom has the possibility to escape from the trap if its total energy E' is larger than the trap depth U'_0 . However, if it is smaller, it will stay in the trap. In order to give the atom the time to leave the trap it is necessary to keep the trap depth at its low level for a time t that is considerably longer than one oscillation period in the trapping potential. After the time t the trap depth is raised back to its initial value U_0 . Then the lasers of the magneto-optical trap are switched on and the presence of the atom in the trap is verified by detection of its fluorescence.

This experimental sequence is repeated many times for a given U'_0 and the probability $p_{det}(U'_0)$ to redetect the atom after the trap depth has been raised back to U_0 is determined. This probability equals the probability that the total energy E' of the atom after the lowering of the trap is smaller than U'_0 :

$$p_{det}(U'_0) = p(E' \leq U'_0) \quad (4.1)$$

By repeating this for different values of U'_0 it is possible to deduce from these measurements the temperature T of the atom. For that one needs a theoretical model

for the dependence of $p(E' \leq U'_0)$ on U'_0 for a given T . The temperature of the atom can then be determined by using T as a fit parameter to fit $p(E' \leq U'_0)$ to the experimentally measured distribution $p_{det}(U'_0)$.

4.2 Theoretical model

In the following calculations the single atom in the optical dipole trap shall be treated as a classical three dimensional harmonic oscillator. For this it has to be assumed that

- (i) The potential of the optical dipole trap is approximately harmonic.
- (ii) The atom follows classical trajectories in the potential and must not be treated as a quantum mechanical oscillator.

The first assumption is justified since the expected temperatures of the atom are on the order of the Doppler temperature $T_{Dop} \approx 146 \mu\text{K}$ [22]. This is ten times lower than the maximal trap depth $U_O = 1.5 \text{ mK}$ so that the atom always remains at the bottom of the trap where the harmonic approximation is valid. For verifying that the second assumption is valid one must compare the eigenenergies of the quantum mechanical oscillator to the thermal energy of the atom. Since the degrees of freedom along the three spatial axes are uncoupled in a three dimensional harmonic oscillator, one can do this for each degree of freedom separately. According to Virial's theorem the mean potential and kinetic energy of a particle in the potential of a harmonic oscillator are the same [46]. For a particle of temperature T with one degree of freedom, E_{pot}^{th} and E_{kin}^{th} are

$$E_{pot}^{th} = E_{kin}^{th} = \frac{1}{2}k_B T \quad (4.2)$$

So the total energy E^{th} in each degree of freedom for a temperature $T = T_{Dop}$ is

$$E^{th} = 2 \cdot \frac{1}{2}k_B T = 2.02 \cdot 10^{-27} \text{ J} \quad (4.3)$$

The eigenenergies $E_n = \hbar\omega(n + \frac{1}{2})$ of a quantum mechanical oscillator are separated by $\hbar\omega$, where ω is the eigenfrequency of the oscillator. With the eigenfrequencies for the oscillations in the radial and longitudinal mode from equations (3.3) and (3.4) one obtains:

$$\begin{aligned} \hbar\omega_r &= 42.08 \cdot 10^{-30} \text{ J} \\ \hbar\omega_l &= 42.20 \cdot 10^{-31} \text{ J} \end{aligned}$$

So at the Doppler temperature the atom is in the $\frac{E^{th}}{\hbar\omega_r} \approx 48$ th excited state of the radial oscillator and the $\frac{E^{th}}{\hbar\omega_l} \approx 495$ th excited state of the longitudinal oscillator,

respectively. This is sufficient to treat the atom as a classical harmonic oscillator.

We now come to the calculation of $p(E' \leq U'_0)$ and start with the probability distributions of the potential and kinetic energy U and E_{kin} of the atom before the trap is lowered. Assuming a classic three-dimensional harmonic oscillator with Boltzmann distribution of the total energy E in each of the three degrees of freedom, the probability distribution of the potential energy is given by [19]

$$p(U) = \frac{2}{\sqrt{\pi}(k_B T)^{3/2}} \sqrt{U} \exp\left(-\frac{U}{k_B T}\right) \quad (4.4)$$

where k_B is the Boltzmann constant. For a harmonic oscillator the distribution of the kinetic energy $E_{kin} = E - U$ is given by the same distribution [19]

$$p(E - U) = \frac{2}{\sqrt{\pi}(k_B T)^{3/2}} \sqrt{E - U} \exp\left(-\frac{E - U}{k_B T}\right) \quad (4.5)$$

Immediately after the lowering of the trap the situation is the following. Since the lowering happens instantaneously the kinetic energy after the lowering is the same as before, so $E'_{kin} = E_{kin}$. Hence, the distribution of the kinetic energy stays the same as well:

$$p(E' - U') = \frac{2}{\sqrt{\pi}(k_B T)^{3/2}} \sqrt{E' - U'} \exp\left(-\frac{E' - U'}{k_B T}\right) \quad (4.6)$$

However, the potential energy is reduced to $U' = x \cdot U$. Thus the distribution of the potential energy is different. It is scaled by a factor of x to lower energies as depicted in figure 4.2. The distribution then is given by

$$p(U') = x^{-1} \frac{2}{\sqrt{\pi}(k_B T)^{3/2}} \sqrt{x^{-1}U'} \exp\left(-\frac{x^{-1}U'}{k_B T}\right) \quad (4.7)$$

where the multiplicative factor x^{-1} is necessary to keep the distribution normalized.

With equations (4.6) and (4.7) it is possible to calculate the probability distribution of the total energy E' immediately after the trap has been lowered. It is given by the convolution of the distributions of U' and E'_{kin}

$$\begin{aligned} p(E') &= \int_0^{E'} p(U') p(E' - U') dU' \\ &= x^{-1} \frac{4}{\pi(k_B T)^3} \int_0^{E'} \sqrt{x^{-1}U'(E' - U')} \exp\left(-\frac{x^{-1}U' + E' - U'}{k_B T}\right) dU' \end{aligned} \quad (4.8)$$

Analytic integration yields:

$$p(E') = \frac{2}{\sqrt{x}(x-1)(k_B T)^2} E' \exp\left(-\frac{E'(x+1)}{2x k_B T}\right) I_1\left(\frac{(x-1)E'}{2x k_B T}\right) \quad (4.9)$$

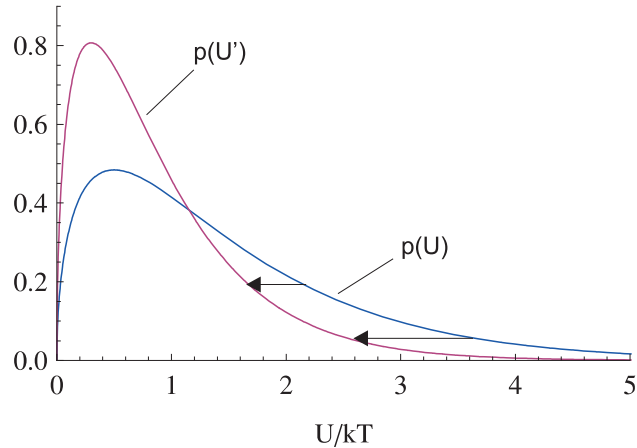


Figure 4.2: Behaviour of the potential energy distribution when the trap depth is instantaneously lowered. The distribution shifts to lower energies.

Where I_1 is the first-order modified Bessel function. The probability that $E' \leq U'_0$ can now be calculated from:

$$p(E' \leq U'_0) = \int_0^{U'_0} p(E') dE' \quad (4.10)$$

It was not possible to solve the integral analytically but this is not absolutely necessary. One can also integrate $p(E' \leq U'_0)$ numerically for different temperatures T . The best fitting parameter T can then be found by graphically comparing plots of $p(E' \leq U'_0)$ with the measured curve of $p_{det}(U'_0)$.

Figure 4.3 shows plots of $p(E' \leq U'_0)$ as a function of U'_0 for different temperatures. One can see that for temperatures below the Doppler temperature $T_{Dop} = 146 \mu\text{K}$ the trap has to be lowered below half of its original depth if one wants to observe considerable atom losses. These plots can now be compared to experimental data.

4.3 Results

Switching of the laser intensity

For lowering and raising the trap depth the intensity of the dipole laser has to be varied. This is realized by adding a negative voltage ΔU_{AOM} to the constant voltage U_{Const} that is applied at the input of the AOM-driver of the dipole laser. A pulse from our pattern generator switches ΔU_{AOM} between $0V$ and the value for which the desired trap depth is obtained. The bandwidth of the electronic circuit that adds ΔU_{AOM} to U_{Const} allows to ramp the trap depth within less than $1\mu\text{s}$. This has to be compared to the cycle durations of one oscillation in the trapping potential. From equations (3.3) and (3.4) one obtains that $T_r \approx 16 \mu\text{s}$ and $T_l \approx 157 \mu\text{s}$ for the radial

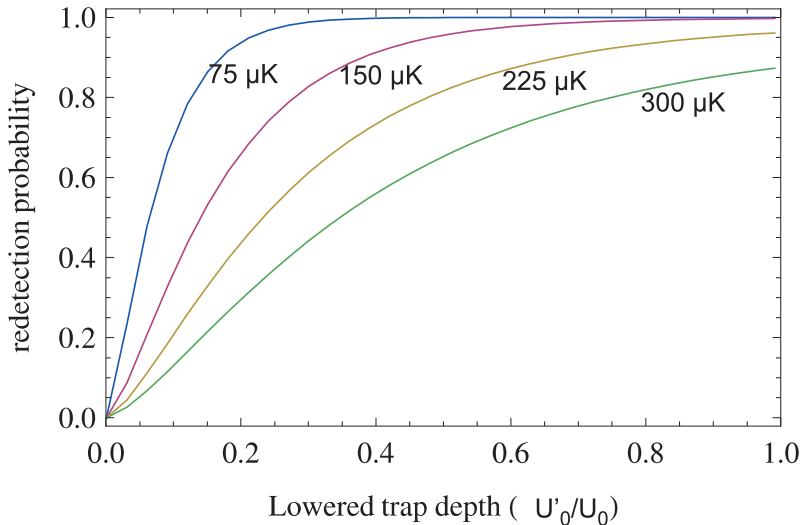


Figure 4.3: Plots of $p(E' \leq U'_0)$ as a function of the lowered trap depth U'_0 for different temperatures.

and longitudinal direction, respectively. So the trap depth can be ramped within a time that is shorter than the shortest possible oscillation period T_r in the trap.

Measurement results and discussion

For measuring the energy distribution of the atoms in the lowered trap potential we scanned the lowered trap depth U'_0 from 0 to $0.3 U_0$ and determined the probability to redetect the atom after the trap potential has been raised to its original depth. The result can be seen in figure 4.4.

The black line shows the measurement result and the red, blue and green lines are theoretical predictions from the model presented in the last section. The red line was calculated for a temperature $T = 57 \mu\text{K}$ and the blue and green lines correspond to $52 \mu\text{K}$ and $62 \mu\text{K}$, respectively. The maximal probability to redetect the atom has been measured to be about 97.5% even if the trap is not lowered at all. This is due to collisions with atoms from the background gas that remove the atom from the trap. The theoretical model has been corrected for this effect.

Above $U'_0 = 0.05 U_0$ the measured curve is in perfect agreement with the theoretical prediction. For lower values the measured curve deviates towards higher redetection probabilities. The explanation for this lies in the time t for which the trap was lowered in this measurement run. It was chosen to be $400 \mu\text{s}$ which is about 2.5 times the period T_l of a longitudinal oscillation for the normal trap depth U_0 . However, when the trap is lowered the periods T_l and T_r increase with $\frac{1}{\sqrt{x}}$ (see equations (3.3) and (3.4)). For $x = 0.03$ the periods are already $T_l \geq 906 \mu\text{s}$ and $T_r \geq 90 \mu\text{s}$, respectively. So the criterion that the trap must be lowered for more

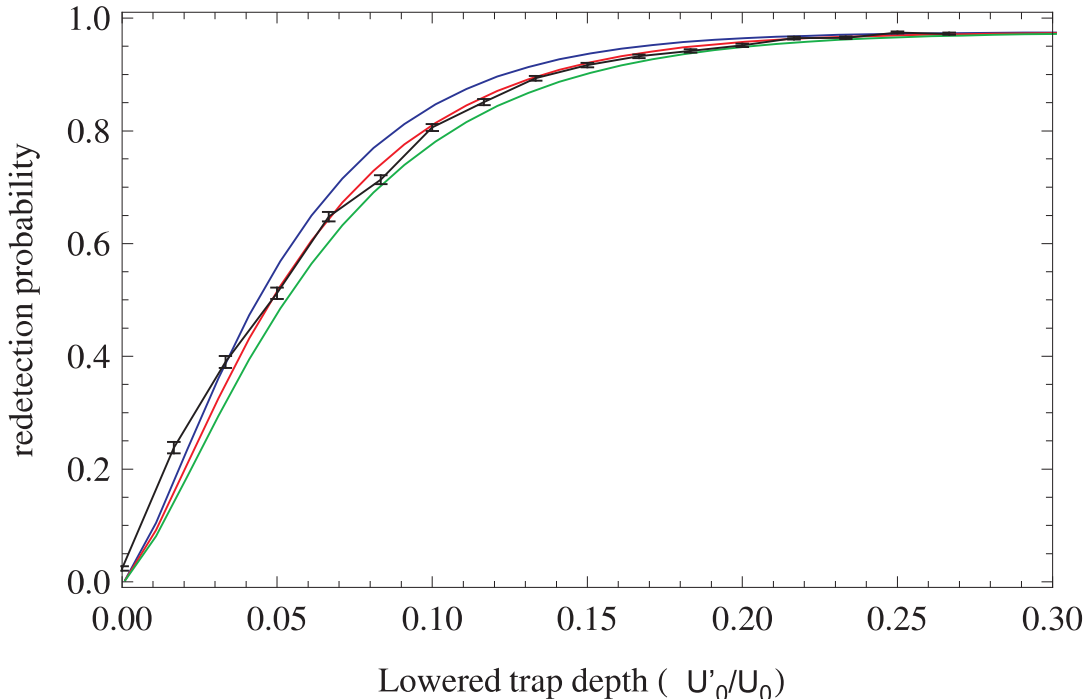


Figure 4.4: Measurement of the total energy distribution of the atom after lowering the maximal trap depth from $U_0 = 1.5 \text{ mK}$ to $U'_0 = x \cdot U_0$. Shown are the measured probabilities $p_{det}(U'_0)$ to redetect the atom after the trap depth has been raised from its lowered depth U'_0 back to its standard value as a function of U'_0 (black line). The red line was calculated with the theoretical model and yields a temperature of the atom of $57 \mu\text{K}$. The blue and green lines correspond to $52 \mu\text{K}$ and $62 \mu\text{K}$, respectively.

than one oscillation period is no more fulfilled and a proportion of the atoms cannot leave the potential. This leads to an increased $p(E')$.

It is probable that this deviation can be avoided by lowering the trap for a longer time. If we neglect it for the moment and consider only the measured line above $U'_0 = 0.05 U_0$ the errors can be determined to be below $\pm 2 \mu\text{K}$.

Summary

This chapter presented a method to measure the temperature of a single neutral atom stored in an optical dipole trap. Starting from the energy distributions of a three-dimensional harmonic oscillator a theoretical model was developed to describe the energy distribution of the atom after the trap potential has been instantaneously lowered. From this a prediction of the probability that the atom is redetected in the trap after it has been ramped back to its original depth was obtained. The theoretical model is in good agreement with the measurement and yields a temperature of the

atom of

$$T = 57 \mu\text{K} \pm 2\mu\text{K} \quad (4.11)$$

which is about $0.42 \cdot T_{Dop}$.

The measured temperature is a clear proof of sub-Doppler cooling effects induced by the cooling beams of the magneto-optical trap. Moreover, the good agreement between the theoretical prediction and experiment shows that the assumption of a Boltzmann distribution of the atomic energy seems to be justified. The presented method is easy to implement compared to methods that are based for example on the precise measurement of the broadening of atomic transition lines where stabilized cavities are needed [27]. Besides the general interest in the thermal properties of a single trapped atom the obtained value of the temperature can also be useful for the calculation of effects of line broadening that occur due to the thermal energy of the atom.

5 Summary and outlook

This work describes the generation and detection of entanglement between a single trapped ^{87}Rb atom and a single photon. Measurements on the atom-photon pair in two complementary bases yielded the non-classical correlations that are typical for entangled systems. From these correlations the fidelity F of the prepared state with respect to the desired $|\Psi^+\rangle$ -state was determined to be 0.745 which is a clear proof of entanglement.

For the readout of the atomic Zeeman state a two-step detection scheme was implemented. First the superposition of Zeeman states is mapped onto a superposition of hyperfine states by means of an adiabatic STIRAP-transfer technique. Then the atom is removed from the trapping potential depending on its hyperfine state. Further optimization should be performed on the transfer efficiency of the STIRAP process that turned out to be the limiting factor for the visibility in the correlation measurements. In order to assure stability of the atomic spin state against dephasing, external magnetic fields have been compensated by an active field stabilization. There is a residual field of ~ 12 mG along the z -axis that shows fluctuations above 200 Hz with a standard deviation of the peak-to-peak amplitude of 2 mG. The atomic qubit is sufficiently stable against dephasing for the duration between the creation of the entangled pair and the atomic state readout. Besides, to increase the repetition rate of the experiment the duration of the optical pumping period has been reduced to $2\ \mu\text{s}$. Furthermore, the efficiency of the excitation process that creates the entangled atom-photon pair was optimized. The total probability to detect one emitted photon per excitation cycle was determined to be $2.2 - 2.4\ \%$.

A first step towards the envisaged entanglement swapping experiment was realized by switching the dipole trap off during the excitation and sponaneous decay of the atom. Thereby it is ensured that the photons originating from the two traps are spectrally indistinguishable. This is a necessary condition for performing a Bell-state measurement by two-photon interference at a beamsplitter.

Apart from realizing atom-photon entanglement a method for measuring the temperature of the single trapped atom was presented. It works by measuring the integrated atomic energy distribution of the atom after the trap depth has been non-adiabatically lowered. A comparison of the measurement with a theoretical model yields a temperature of the single atom of $57 \pm 2\ \mu\text{K}$ which is well below the Doppler temperature of ^{87}Rb .

All in all it can be concluded that during this work the second single atom trap

has reached a stage similar to the first setup.

Outlook

As a next step towards entanglement swapping between the remotely trapped atoms, two-photon interference at a beamsplitter must be realized. For this it is necessary to synchronize the creation of the photons in the two traps such that they arrive at the beamsplitter simultaneously. Therefore the pattern generators for creating the laser pulses are clocked by a common frequency generator. This allows to reduce the time jitter between the excitation pulses that create the photons below 1 ns. Furthermore, a 30 m optical fiber link between the two laboratories has been set up that will be used to transmit the photons from the second trap to the first one where the Bell-state measurement will take place. To avoid random rotations of the polarization state of the photon propagating in the fiber the optical link has to be stabilized with the polarization control setup demonstrated in [26, 15].

In order to be able to close the locality loophole in a test of Bell's inequality a faster atomic state detection is being developed. Similiar to the current scheme a STIRAP-transfer first distinguishes between orthogonal superpositions of Zeeman states. However, the hyperfine state detection which is currently based on fluorescence detection will be replaced by a faster scheme based on state selective ionization of the atom and detection of the ionization fragments. First measurements show that the atom can be ionized with a probability of 96 % within 350 ns [47]. The ionization fragments are then detected with two channel-electron mulitpliers about 400 ns after the ionization. The probability for detecting either the electron or the ion or both fragments was determined to be $\sim 95 - 98\%$ [48]. Moreover, the selection of the atomic measurement basis will also be replaced by a faster one. Currently this is done by rotating λ -waveplates that are mounted on stepper motors. In future an electro-optical modulator (EOM) will be used that allows to modulate the polarization of the STIRAP beam with a bandwidth of 100 MHz.

All in all it will be possible to perform the atomic state reaout including the choice of the measurement basis within less than $1 \mu s$. Together with the aimed distance between the atoms of 300 m this will allow a test of Bell's inequality with the locality loophole as well as the detection loophole closed.

A Appendix

A.1 Rubidium 87 data

- Atomic mass m : $1.443 \cdot 10^{-25}$ kg
- Nuclear spin I : $3/2$

D₂-line data ($5^2S_{1/2} \rightarrow 5^2P_{3/2}$)

Frequency	ω_0	$2\pi \cdot 384.2$ THz
Wavelength	λ	780.241 nm
Lifetime	τ	26.23 ns
Decay Rate/ Natural linewidth (FWHM)	Γ	$38.12 \cdot 10^6 s^{-1}$ $2\pi \cdot 6.067$ MHz
Doppler temperature	T_{Dop}	145.57 μ K
Transition Dipole matrix element	$\langle J = 1/2 er J' = 3/2 \rangle$	$3.584 \cdot 10^{-29} C \cdot m$

D₁-line data ($5^2S_{1/2} \rightarrow 5^2P_{1/2}$)

Frequency	ω_0	$2\pi \cdot 377.1$ THz
Wavelength	λ	794.978 nm
Lifetime	τ	27.68 ns
Decay Rate/ Natural linewidth (FWHM)	Γ	$36.129 \cdot 10^6 s^{-1}$ $2\pi \cdot 5.75$ MHz
Transition Dipole matrix element	$\langle J = 1/2 er J' = 1/2 \rangle$	$2.538 \cdot 10^{-29} C \cdot m$

A.2 Saturation intensities

The saturation intensity I_{sat} of a dipole transition line between the Zeeman ground state $5^2S_{1/2}, F, m_F$ and the excited state $5^2P_{x/2}, F', m'_F$ ($x \in \{1, 3\}$) is given by [22]:

$$I_{sat} = \frac{c\epsilon_0\Gamma^2\hbar^2}{4|\langle J||er||J'\rangle \cdot \text{CGC}(F, m_F; F', m'_F)|^2} \quad (\text{A.1})$$

Where ϵ_0 is the permittivity of vacuum. Γ is the decay rate of the respective transition line (D_1 or D_2 in our cases). And $\langle J||er||J'\rangle$ is the transition dipole matrix element of the respective transition line (see tables in A.1). Moreover, $\text{CGC}(F, m_F; F', m'_F)$ is the Clebsch-Gordon coefficient of the considered transition.

From equation (A.1) the saturation intensities of the transitions used in the experiment can be calculated with the Clebsch-Gordon coefficients given in [22]:

Excitation	5.0079 $\frac{\text{mW}}{\text{cm}^2}$
Pump 1	33.386 $\frac{\text{mW}}{\text{cm}^2}$
Pump 2	4.0063 $\frac{\text{mW}}{\text{cm}^2}$
Push-out	1.669 $\frac{\text{mW}}{\text{cm}^2}$
STIRAP 1	5.983 $\frac{\text{mW}}{\text{cm}^2}$
STIRAP 2	17.95 $\frac{\text{mW}}{\text{cm}^2}$

Table A.1: Saturation intensities for the transitions used in experiment

Bibliography

- [1] A. Einstein; B. Podolsky; N. Rosen. Can quantum-mechanical description of physical reality be considered complete? *Phys. Rev.*, 47:777780, 1935.
- [2] D. Bohm. *Quantum Theory*. Prentice-Hall, Englewood Clis, New York, 1951.
- [3] J.S. Bell. On the Einstein-Podolsky-Rosen paradox. *Physics*, 1:195200, 1964.
- [4] S.J. Freedman; J.F. Clauser. Experimental test of local hidden-variable theories. *Phys. Rev. Lett.*, 28:938, 1972.
- [5] A. Aspect; P. Grangier; and Gérard Roger. Experimental tests of realistic local theories via Bell's theorem. *Phys. Rev. Lett.*, 47:460, 1981.
- [6] A. Aspect; P. Grangier; and Gérard Roger. Experimental realization of Einstein-Podolsky-Rosen-Bohm gedankenexperiment: A new violation of Bell's inequalities. *Phys. Rev. Lett.*, 49:9194, 1982.
- [7] A. Aspect; J. Dalibard; Gérard Roger. Experimental test of Bell's inequalities using time-varying analyzers. *Phys. Rev. Lett.*, 49:1804, 1982.
- [8] G. Weihs; T. Jennewein; C. Simon; H. Weinfurter; A. Zeilinger. Violation of Bell's inequality under strict Einstein locality conditions. *Phys. Rev. Lett.*, 81:5039, 1998.
- [9] M.A. Rowe; D. Kielpinsky; V. Meyer; C.A. Sacket; W.M. Itano; C.Monroe; D.J. Wineland. Experimental violation of Bell's inequality with efficient detection. *Nature*, 409:791–794, 2001.
- [10] D.N. Matsukevich; P.Maunz; D.L. Moehring; S. Olmschenk; and C. Monroe. Bell inequality violation with two remote atomic qubits. *Phys. Rev. Lett.*, 100:150404, 2008.
- [11] D. Bouwmeester; A. Ekert; A. Zeilinger. *The physics of quantum information*. Springer-Verlag, Berlin, 2000.
- [12] M.A. Horne M. Zukowski, A. Zeilinger and A.K. Ekert. "Event-ready-detectors" Bell experiment via entanglement swapping. *Phys. Rev. Lett.*, 71:4287, 1993.

- [13] D. Bruß; G. Leuchs. *Lectures on quantum information*. Wiley-VHC, Weinheim, 2007.
- [14] J. Volz; M. Weber; D. Schlenk; W. Rosenfeld; J. Vrana; K. Saucke; C. Kurtsiefer; H. Weinfurter. Observation of entanglement of a single photon with a trapped atom. *Phys. Rev. Lett.*, 96:030404, 2006.
- [15] W. Rosenfeld; F. Hocke; F. Henkel; M. Krug; J. Volz; M. Weber; H. Weinfurter. Towards long-distance atom-photon entanglement. *Phys. Rev. Lett.*, 101:260403, 2008.
- [16] M. Krug. Atomic traps for efficient state detection of a single atom. Master's thesis, Ludwig-Maximilians-Universität München, 2007.
- [17] Ch. Jakob. Zustandspräparation einzelner Atome. Master's thesis, Ludwig-Maximilians-Universität München, 2008.
- [18] A. Deeg. Zustandsdetektion eines einzelnen Atoms. Master's thesis, Ludwig-Maximilians-Universität München, 2008.
- [19] W. Rosenfeld. *Experiments with an entangled system of a single atom and a single photon*. PhD thesis, Ludwig-Maximilians-Universität München, 2008.
- [20] I.L. Chuang M.A. Nielsen. *Quantum Computation and Quantum Information*. Cambridge University Press, Cambridge, 2000.
- [21] A. Peres. Separability criterion for density matrices. *Phys. Rev. Lett.*, 77:1413, 1996.
- [22] Daniel A. Steck. Rubidium 87 D line data. *available online at <http://steck.us.alkalidata> (revision 2.1, 1 September 2008)*.
- [23] J.D. Jackson. *Classical Electrodynamics*. Wiley, New York, 1962.
- [24] D. Schlenk. Atom-Photon Verschränkung. Master's thesis, Ludwig-Maximilians-Universität München, 2004.
- [25] T. Legero; T. Wilk; A. Kuhn; G. Rempe. Characterization of single photons using two-photon interference. *arXiv:0512023*, 2005.
- [26] F. Hocke. Long-distance atom-photon entanglement. Master's thesis, Ludwig-Maximilians-Universität München, 2007.
- [27] J. Volz. *Atom-photon entanglement*. PhD thesis, Ludwig-Maximilians-Universität München, 2006.

-
- [28] J.F. Clauser; M.A. Horne; A. Shimony; R.A. Holt. Proposed experiment to test local hidden-variable theories. *Phys. Rev. Lett.*, 23:880884, 1969.
- [29] P.M. Pearle. Hidden-variable example based upon data rejection. *Phys. Rev. D*, 2:1418, 1970.
- [30] A.E. Lita; A.J. Miller; Sae Woo Nam. Counting near-infrared single-photons with 95% efficiency. *Optics Express*, 16:3032–3040, 2008.
- [31] W. Rosenfeld; M. Weber; J. Volz; F. Henkel; M. Krug; A. Cabello; M. Zukowski; H. Weinfurter. Towards a loophole-free test of Bell’s inequality with entangled pairs of neutral atoms. *arXiv:0906.0703*, 2009.
- [32] B.B. Blinov; D.L. Moehring; L.-M. Duan; C. Monroe. Observation of entanglement between a single trapped atom and a single photon. *Nature*, 428:153, 2004.
- [33] L. Ricci; M. Weidemüller; T. Esslinger; A. Hemmerich; C. Zimmermann; V. Vuletic; W. König; T.W. Hänsch. A compact grating-stabilized diode laser system for atomic physics. *Optics Communications*, 117:541–549, 1995.
- [34] K. Kurtsiefer. A programmable pattern generator.
- [35] H. J. Metcalf; P. van der Straten. *Laser cooling and trapping*. Springer Verlag, New York, 1999.
- [36] J. Dalibard; C. Cohen-Tannoudji. Laser cooling below the doppler limit by polarization gradients: Simple theoretical models. *J. Opt. Soc. Am. B*, 6:20232045, 1989.
- [37] R. Grimm; M. Weidemüller; Y. Ovchinnikov. Optical dipole traps for neutral atoms. *arXiv:physics/9902072v1*, 1999.
- [38] T. Laine; S. Stenholm. Adiabatic processes in three-level systems. *Phys. Rev. A*, 53:2501–2512, 1996.
- [39] M.O. Scully; M.S. Zubairy. *Quantum Optics*. Cambridge University Press, 1997.
- [40] C. Cohen-Tannoudji; J. Dupont-Roc; G. Grynberg. *Atom-Photon interactions*. Wiley-Interscience, 1998.
- [41] M. Weber. *private communication*. 2009.

- [42] J. Beugnon; M.P.A. Jones; J. Dingjan; B. Darquié; A. Browaeys; P. Grangier. Quantum interference between two single photons emitted by independently trapped atoms. *Nature*, 440:779, 2006.
- [43] T. Legero; T.Wilk; M. Hennrich; G.Rempe; A.Kuhn. Quantum beat of two single photons. *Phys. Rev. Lett.*, 93:070503, 2004.
- [44] W. Alt; D. Schrader; S. Kuhr; M. Müller; V. Gomer; D. Meschede. Single atoms in a standing-wave dipole trap. *Phys. Rev. A*, 67:033403, 2003.
- [45] C. Tuchendler; A.M. Lance; A. Browaeys; Y. Sortais; P. Grangier. Energy distribution and cooling of a single atom in an optical tweezer. *arXiv:0805.3510*, 2008.
- [46] Landau; Lifschitz. *Mechanik (Lehrbuch der theoretischen Physik, Band 1)*. Deutsch, Frankfurt a. Main, 2004.
- [47] M. Krug. *private communication*. 2009.
- [48] F. Henkel. *private communication*. 2009.

Danksagungen

Zu guter Letzt noch ein herzlicher Dank an all diejenigen, die physikalisch oder auch moralisch zum Gelingen dieser Arbeit beigetragen haben:

- Professor Harald Weinfurter für die Aufnahme in seine Arbeitsgruppe und das freie und kreative Arbeitsumfeld.
- Markus Weber für die tolle Unterstützung, die Ermutigungen in harten Zeiten und dafür, dass er mit seinem österreichischen Charme stets dafür sorgt, dass der Gruppe nie der Elan ausgeht.
- Wenjamin Rosenfeld für seine Anstrengungen mir möglichst schnell einen tiefen Einblick in das Experiment zu geben. Von ihm habe ich gelernt, dass sich für sehr viel mehr Dinge eine einfache logische Erklärung finden lässt, als man denkt. Das ermutigt auch öfter selbst mal nachzuhaken...
- Michael Krug für die schönen gemeinsamen Stunden beim Justieren und Messen. Der Soundtrack dazu hätte nicht besser sein können.
- Florian Henkel für sein Durchhaltevermögen bei der Entwicklung der neuen Detektoren. Herzlichen Glückwunsch schon mal für die tollen Ergebnisse.
- Julian Hofmann für die nette Büro-WG und die ersten gemeinsamen Monate im Labor.
- Daniel Schlenk für den festen Schuß. Und dafür, dass er kein Atomi ist. Das brachte mal etwas Farbe in die Mittagspausen
- Meinen Eltern, die mir dieses Studium und alles rundherum ermöglicht haben, sowie meinem Bruder Christian für die vielen schönen Tage in den Bergen.
- Meinen Freunden aus dem Studium, mit denen zusammen ich mir einen Zugang zur Physik erarbeitet habe. Ohne sie wäre ich nicht so weit gekommen.
- Der Wohnheimsiedlung Maßmannplatz und ihren Bewohnern. Was ich von dort an Erinnerungen und Erfahrungen mitnehme ist einfach unersetzlich.
- Dorothée für ihr strahlendes Lächeln und ihre Geduld in schwierigen Zeiten.

Hiermit versichere ich, daß ich die vorliegende Arbeit selbständig und nur unter Verwendung der angegebenen Quellen und Hilfsmittel verfaßt habe.

München, den 06. Juli 2009